

1 **The occipital place area is recruited for echo-acoustically guided navigation in**
2 **blind human echolocators**

3 Abbreviated title: Occipital place area and echo-acoustic navigation

4

5 Authors: Liam J. Norman¹ and Lore Thaler¹

6 ¹*Department of Psychology, Durham University, Durham, DH1 3LE*

7

8 *Correspondence:*

9 *Liam J. Norman (liam.norman@durham.ac.uk), Lore Thaler (lore.thaler@durham.ac.uk)*

10

11 Length: Abstract (232 words), significance (103 words), introduction (646 words), discussion
12 (1,496 words), 11 figures, 6 tables

13

14 Conflict of interest statement: The authors declare no conflicts of interest

15 Acknowledgements: This work was supported by a UKRI Biotechnology and Biological
16 Sciences Research Council Grant BB/M007847/1 to LT.

17

18 For the purpose of open access, the authors have applied a Creative Commons Attribution
19 (CC BY) licence to any Author Accepted Manuscript version arising

20

21

22

23 Abstract

24 In the investigation of the brain areas involved in human spatial navigation, the traditional
25 focus has been on visually guided navigation in sighted people. Consequently, it is unclear
26 whether involved areas also support navigational abilities in other modalities. We explored
27 this possibility by testing whether the occipital place area (OPA) – a region associated with
28 visual boundary-based navigation in sighted people – has a similar role in echo-acoustically
29 guided navigation in blind human echolocators. We used fMRI to measure brain activity in
30 six blind echolocation experts (EEs; 5 males, 1 female), twelve blind controls (BCs; 6 males, 6
31 females), and fourteen sighted controls (SCs; 8 males, 6 females) as they listened to pre-
32 recorded echolocation sounds that conveyed either a route taken through one of three maze
33 environments, a scrambled (i.e. spatiotemporally incoherent) control sound, or a no-echo
34 control sound. We found significantly greater activity in the OPA of EEs, but not the control
35 groups, when they listened to the coherent route sounds relative to the scrambled sounds.
36 This provides evidence that the OPA of the human navigation brain network is not strictly tied
37 to the visual modality but can be recruited for non-visual navigation. We also found that EEs,
38 but not BCs or SCs, recruited early visual cortex for processing of echo-acoustic information.
39 This is consistent with the recent notion that the human brain is organised flexibly by task
40 rather than by specific modalities.

41 **Keywords: audition, fMRI, route recognition**

42

43 **Significance statement**

44 There has been much research on the brain areas involved in visually guided navigation, but
45 we do not know whether the same or different brain regions are involved when blind people
46 use a sense other than vision to navigate. In this study, we show that one part of the brain
47 (occipital place area) known to play a specific role in visually guided navigation is also active
48 in blind human echolocators when they use reflected sound to navigate their environment.
49 This finding opens up new ways of understanding how people navigate, and informs our
50 ability to provide rehabilitative support to people with vision loss.

51 Introduction

52 Human spatial navigation involves a network of brain areas, reflecting the different
53 components involved in navigation (Ekstrom *et al*, 2017; Kong *et al*, 2017; Boccia *et al*, 2014).
54 What is unclear, however, is whether these areas serve a role that is specific to whichever
55 modality is most dominantly used for navigation (typically vision in humans), or whether they
56 serve a more general role that could accommodate another modality entirely. Indeed, there
57 is an increasing amount of evidence to suggest that the human brain is organised flexibly by
58 task rather than by sensory modality (Amedi *et al*, 2017) – that is, a given brain area can
59 serve the same function across different input modalities.

60 Visual perception has been at the forefront of navigation research in humans due to the
61 uniquely salient role of visual information (Ekstrom *et al*, 2017; Chan *et al*, 2012; Ekstrom
62 2015). That is not to say, however, that non-visual information could also be used. For
63 example, people who are blind are also capable of excellent spatial navigation (Thinus-Blanc
64 & Gaunet, 1997; Loomis *et al*, 2001). Rather, it is poorly understood whether such non-
65 visual navigational abilities involve the same brain processes as visual-based navigation
66 (Fiehler *et al*, 2015; Kupers *et al*, 2010; Maidenbaum, Chebat & Amedi, 2018).

67 In order to address this, we must identify whether brain areas with specific roles in visual-
68 based navigation have equivalent roles during non-visual navigation. One brain region in
69 particular – the occipital place area (OPA) – is known to provide the perceptual source of
70 environmental boundary information that guides navigation through that environment
71 (Kamps *et al*, 2016; Julian *et al*, 2016). Furthermore, because the OPA it is located near the
72 transverse occipital sulcus, it is assumed that this perceptual representation emerges from
73 visual input. Human echolocation offers a well-suited model in which to test whether the
74 OPA has a similar navigational role in a non-visual modality. Echolocation is the ability to
75 perceive objects and space through sound echoes (Griffin, 1944) and offers the ability to
76 perceive the proximal and distal environment. Some people who are blind use click-based
77 echolocation (i.e. echolocation using mouth-clicks) to perceive an object’s position in space
78 as well as its shape, material, and whether it is in motion (for reviews see Kolarik, *et al*, 2014;
79 Thaler & Goodale, 2016). Furthermore, using echolocation for these purposes is associated
80 with neural activity in areas that are typically associated with perceiving those same
81 properties through vision (Norman & Thaler, 2019; Thaler *et al*, 2011; Arnott *et al*, 2013;
82 Milne *et al*, 2015; Thaler *et al*, 2014).

83

84 We used fMRI to measure brain activity in 6 blind echolocation experts (EEs), 12 blind
85 controls (BCs), and 14 sighted controls (SCs) as they listened to pre-recorded binaural
86 echolocation sounds (i.e. echo-acoustic sound through a first-person perspective) and made
87 perceptual judgments about them. The critical contrast in our analysis was to compare brain
88 activity during coherent route sounds to activity during scrambled (i.e. spatiotemporally
89 incoherent) sounds. This design is an echo-acoustic analogue of one used previously to
90 identify OPA activity during visually guided navigation (Kamps *et al*, 2016).

91 We used a region of interest (ROI) analysis approach, focussing on the OPA in addition to the
92 parahippocampal place area (PHPA) because of its role in the neural representation of places
93 and scenes (Epstein *et al*, 1999), and the superior parietal lobule (SPL) because of its
94 previously identified activation in some non-visual navigation tasks (Kupers *et al*, 2010;
95 Fiehler *et al*, 2015). We also included ROIs for primary visual and auditory areas (V1 and A1,
96 respectively) to analyse activity in low-level sensory processing areas, and also because there
97 is some evidence that V1 is active during non-visual navigation (Maidenbaum *et al*, 2018). In
98 addition to the ROI analysis, we also ran a whole-brain analysis.

99 Part of the data (behavioural performance outside the scanner for SCs and three EEs) has
100 been reported previously (Dodsworth *et al*, 2020).

101

102 Materials and Methods

103 Ethics

104 All Procedures followed the British Psychological Society code of practice and the World
105 Medical Association's Declaration of Helsinki. The experiment had received ethical approval
106 by the Ethics Advisory Sub-Committee in the Department of Psychology at Durham University
107 (Ref 14/13). All participants gave written informed consent to take part in this study.
108 Participants who were sighted and participants who were blind received £6/hr and £10/hr,
109 respectively, to compensate them for their effort and time taking part.

110

111 Participants

112 All participants were recruited through word of mouth and opportunity sampling. Six blind
113 expert echolocators (EEs; 5 males, 1 female) took part (details given in Table 1). Our
114 requirements for classing an individual as an echolocation expert were that they reported
115 using click-based echolocation on a daily basis for more than 10 years. In our sample, five out
116 of the six EEs (EEs) had cause of vision loss present from birth and were diagnosed as legally
117 blind from birth/within the first year of life. The remaining EE (EE4) received an official
118 diagnosis age 12 due to sudden vision loss. Thus, the majority of our echolocation expert
119 participants are classified as early blind.

120

121 <Table 1>

122

123 Twelve blind participants (BCs; 6 males, 6 females) with no prior experience in click-based
124 echolocation took part (details shown in Table 1). In our sample, all BCs had cause of vision
125 loss present from birth. All were diagnosed as legally blind in childhood, with only two official
126 diagnoses at an age that might have coincided with onset of puberty, or may have been after
127 onset of puberty (i.e. 13 yrs and 10 yrs; BC9 and BC2), but again with vision impairment
128 having been present from birth. Thus, the majority of our participants were classified as early
129 blind. All our blind participants were independent travellers, and all had received mobility
130 and orientation training as part of visual impairment (VI) habilitation and VI rehabilitation
131 that is provided to people with VI in the UK. Fourteen sighted participants (SCs; 8 males, 6
132 females) took part (ages: 21, 21, 22, 22, 23, 24, 25, 27, 32, 35, 38, 48, 60, and 71; mean =
133 33.5, SD = 15.8, median = 26). All reported to have normal or corrected to normal vision and
134 no prior echolocation experience (based on self-report).

135

136 All participants had normal hearing appropriate for their age group (ISO 7029:2017) as
137 assessed using pure tone audiometry, with the exception of one blind participant (BC6, aged
138 72 yrs) who wore hearing aids to compensate for age related hearing loss. For purposes of
139 testing, the participant with hearing aids did not wear their aids during any of the
140 experimental testing sessions, as they would not be able to wear these in the MRI scanner.
141 For our statistical analyses that involve comparisons to the BC group, we report the results of
142 those analyses both with and without BC6 included. All participants who had any residual
143 vision were tested under blindfold.

144

145 Experimental design and statistics

146 The design contained a between-subject variable (subject group) and within-subject variable
147 (sound stimulus). Full details of the statistical analyses of the behavioural, ROI, and whole-
148 brain data are given in the relevant sections below. To summarise briefly, behavioural and
149 ROI data was analysed using ANOVAs and Kruskal-Wallis tests and, where appropriate, one-
150 sample t tests and Wilcoxon signed-rank tests. The issue of multiple comparisons was
151 addressed using either Bonferonni correction or the Benjamini-Hochberg method. Whole-
152 brain fMRI data was analysed using ANOVAs and one-sample t tests, with cluster-based
153 thresholding and Gaussian random field correction (Worsley, 2001).

154

155 Echolocation stimuli

156 The stimuli were created from a large set of recordings first described by Dodsworth, Norman
157 & Thaler (2020). For full details of those stimuli, please refer to that report. Briefly, binaural

158 recordings of clicks and click-echoes were made with an anthropometric manikin in physical
159 spaces comprising corridors in specific spatial arrangements (T-mazes, U-mazes, Z-mazes).
160 Details of the manikin have been reported in (Norman & Thaler, 2018). In addition, we also
161 created spatially mirrored versions of these recordings by flipping the left and right channels,
162 giving six maze layouts in total.

163

164 For each of the six mazes, we created two samples by selecting recordings corresponding to a
165 specific sequence of locations and orientations within that maze (see figure 1). This gave a
166 total of 12 sound files that were each 10.53 s in length and contained 18 clicks and echoes,
167 each separated by 600 ms (a rate of 1.71 clicks/s). These 12 sound files were assigned to one
168 of three categories: (1) single-turn route, (2), two-turn route in same direction, (3), two-turn
169 route in different (opposite) directions.

170

171 In addition to these spatially coherent route sounds, we created two types of control sounds:
172 scrambled route sounds and clicks with no echoes. A scrambled route sound was created for
173 each of the original route sounds in order to create sounds that had exactly the same low-
174 level acoustic information (i.e. timing, clicks and echoes), but did not convey spatially
175 coherent information. To do this, the individual click-echo sounds in each route sound file
176 were randomly shuffled and pieced together (maintaining the same click rate) so that there
177 was no coherent route. In order to create a secondary set of control stimuli (i.e. stimuli with
178 clicks but not containing any echoes), a sound recording was used during which the manikin
179 had been placed facing the foam padded wall in the anechoic chamber. The sound was then
180 repeated at the same temporal sequence as that for the 'route' and 'scrambled' sound files.

181

182 <Figure 1>

183

184 In total, five types of sound stimuli were created: single-turn route, two-turns-same route,
185 two-turns-different route, scrambled route, and click only. Example .wav files for each of
186 these stimuli can be found on Open Science Framework: <https://osf.io/c5pn2/>, but note that
187 playback of these example sounds should be done using a high-spec sound card and
188 headphones, due to the nature of the echolocation sounds.

189

190 Stimuli containing echoes ('route' and 'scrambled' stimuli) were of higher root mean square
191 (RMS) intensity than stimuli not containing echoes ('no echo'). Specifically, T and T-
192 scrambled sounds: -41.4 dB; U and U scrambled sounds: -41.4 dB; Z and Z-scrambled
193 sounds: -40.8 dB; No echo sounds: -44.2 dB). In terms of absolute intensity at which sounds
194 were played, each participant selected a sound intensity that felt comfortable for them to do
195 the task. The same intensity was maintained for that participant throughout testing.
196 Recorded sound files were filtered to achieve frequency response equalisation for playback
197 through the MRI-compatible insert earphones (Model S-14, Sensimetrics, Malden, MA; filters
198 provided by the manufacturer).

199

200 Behavioural paradigm before fMRI scanning

201 On a separate day before fMRI scanning, participants completed two runs of 30 trials. On
202 each trial they heard one of the sound stimuli from one of the five categories (single-turn
203 route, two-turns-same route, two-turns-different route, scrambled, and no echo), with each
204 condition being repeated six times. The order of trials was randomly determined at the start

205 of each run. When the sound finished playing, participants gave a verbal response to indicate
206 which category the sound belonged to. The experimenter recorded this response and
207 started the next trial. Before participants performed the two runs of 30 trials, they were
208 played two examples for each type of sound to make them familiar with the sounds and the
209 required responses.

210

211 Setup and apparatus before fMRI scanning

212 Participants completed the task in a sound-insulated and echo-acoustic dampened room
213 (approx. 2.9 m × 4.2 m × 4.9 m) lined with foam wedges (cut-off frequency 315 Hz) in the
214 Department of Psychology at Durham University. Sounds were played through MRI-
215 compatible insert earphones (Model S-14, Sensimetrics, Malden, MA; filters provided by the
216 manufacturer) encased in disposable foam tips (the earphones provided a 20 to 40-dB
217 attenuation level information). These earphones were amplified by a Kramer 900N Stereo
218 Power Amplifier (Kramer Electronics Ltd., Jerusalem, Israel), with input provided by a USB
219 Soundcard (Creative Sound Blaster X-Fi HD Sound Card; Creative Technology Ltd., Creative
220 Labs Ireland, Dublin, Ireland). The experimenter used a laptop (Dell Latitude E7470; Intel
221 Core i56300U CPU 2.40; 8GB RAM; 64-bit Windows 7 Enterprise) running MATLAB R2018b
222 (The Mathworks, Natick, MA) and modified functions from the Psychtoolbox library (Brainard,
223 1997) to control sound playback and to record participants' responses.

224

225 Behavioural paradigm during fMRI scanning

226 Participants' task inside the scanner was the same as that outside the scanner, with some
227 modifications. Participants gave their response after each stimulus presentation by pressing
228 one of five buttons on an MR compatible response unit (5-Button Fibre Optic Response

229 Button System, Psychology Software Tools, Inc, Pittsburgh, USA). Each finger was assigned a
230 different response (thumb = no echo, index = single-turn, middle = two-turns-same, ring =
231 two-turns-different, pinkie = scrambled). A beep (1.2 kHz, 50 ms) at the end of stimulus
232 presentation prompted participants to respond. In addition to the five stimulus categories, a
233 sixth “silence” category was also used (to allow comparisons to baseline activity in the fMRI
234 data analysis). During these silence trials, no sound was played to participants and no
235 response was required. The order of stimulus presentation was counterbalanced with respect
236 to the three main stimulus conditions (route, scrambled, and no echo). This was achieved by
237 breaking down 36 trials in each run into nine sequential groups of four. The first trial in each
238 group was always a silence trial, and the remaining three were a random order of route,
239 scrambled, and no echo. The order of these three trial types was counterbalanced such that
240 after every two runs, each type was presented equally often in each of the three sequence
241 positions. The same randomised order of sounds was used for all participants.

242

243 Setup and apparatus during fMRI scanning

244 All MR data were acquired at Durham University Centre for Imaging (James Cook University
245 Hospital, Middlesbrough, UK), with a 3-Tesla, whole-body MRI system (Magnetom Tim Trio;
246 Siemens, Erlangen, Germany) and 32-channel head coil. For sound presentation the same
247 equipment as that used before fMRI scanning was used to play sounds, with the exception
248 that a PC (Intel Core i7-6700 CPU 3.40; 8GB RAM; 64-bit Windows 7 Enterprise) was used
249 instead of a laptop. Further, participants gave their response using an MRI-compatible 5-
250 button fibre-optic button response unit (Psychology Software Tools, Inc., Pittsburgh, USA)
251 with their right hand. To minimize background noise, the MRI bore’s circulatory air fan was
252 turned off during experimental runs. To minimise interference from light sources, all lights

253 inside the MRI room were turned off and participants who were not totally blind wore a
254 blindfold.

255

256 fMRI scanning parameters

257 High-resolution structural images for each participant were acquired using a T1-weighted,
258 optimised sequence (MP RAGE), at a resolution of 1 x 1 x 1 mm. Functional images were
259 acquired using a single-shot gradient echo-planar pulse sequence in combination with a
260 sparse sampling design (Hall *et al*, 1999), with a repetition time of 13 seconds (11 seconds of
261 inactivity for stimulus presentation, followed by 2 seconds of volume acquisition). Thus,
262 during stimulus presentation, no functional volumes were acquired. Instead, a single
263 functional volume was acquired in the 2-s period after the end of stimulus presentation. Field
264 of view was 192 mm with a matrix size of 64 x 64, giving an in-slice resolution of 3 mm. 38
265 contiguous axial slices were acquired in ascending order with a slice thickness of 3.5 mm,
266 covering the whole brain. Echo time was 30 ms and flip angle was 90°. For each run, a total
267 of 38 functional volumes were acquired, with each run lasting 8 minutes and 14 seconds.
268 The first and last volume in each run were acquired after silence. A total of six runs were
269 completed per participant, except for one participant (EE2) where only four runs were
270 completed.

271

272 fMRI data processing

273 fMRI data pre-processing and analysis was carried out using FEAT (fMRI Expert Analysis Tool)
274 Version 6.00, part of FSL (FMRIB's Software Library, www.fmrib.ox.ac.uk/fsl); Woolrich, Ripley,
275 Brady & Smith, 2001; Woolrich, Behrens, Beckmann, Jenkinson, & Smith, 2004).

276

277 Images were brain-extracted (using BET; Smith, 2002) and within-participant registration of
278 low-resolution functional images to high-resolution structural (T1) images was achieved using
279 FLIRT (6 d.f.; Jenkinson, Bannister, Brady, & Smith, 2002; Jenkinson & Smith, 2001). Further
280 non-linear registration to MNI152 standard space (voxel size of 2 mm) was achieved using
281 FNIRT (Andersson, Jenkinson & Smith, 2020) with a warp resolution of 2 mm. The very first
282 functional volume within each run was discarded, leaving 37 volumes to analyse, the first and
283 last of which were acquired after silence. The following pre-statistic processing was applied
284 to each run of functional data: slice-timing correction using Hanning-windowed sinc
285 interpolation, motion correction using MCFLIRT (Jenkinson *et al*, 2002), high-pass temporal
286 filtering (maximum allowed period = 100 s, or 0.01 Hz), and spatial smoothing (full-width at
287 half maximum Gaussian kernel of 5 mm).

288

289 fMRI modelling and contrasts

290 In the first-level analysis for each run, three explanatory variables (EVs) were modelled using
291 stick function regressors (with no haemodynamic response convolution, due to the sparse
292 sampling design): route stimulus, scrambled stimulus, and no-echo stimulus. The silence trials
293 were used as an implicit baseline. These EVs were then used to define the three contrasts of
294 interest: route vs. scrambled (EV weights: route = +1, scrambled = -1, no echo = 0), echo vs.
295 no echo (EV weights: route = +1, scrambled = +1, no echo = -2), and sound vs. silence (EV
296 weights: route = +1, scrambled = +1, no echo = +1).

297

298 In a second-level analysis stage, single-participant activations across all runs were calculated
299 using a fixed effects model, by forcing the random effects variance to zero in FLAME (FMRIB's
300 Local Analysis of Mixed Effects; Beckmann, Jenkinson & Smith, 2003, Woolrich, *et al* 2004,

301 Woolrich 2008). In a higher-level analysis stage, group-level activations were calculated using
302 a mixed effects model.

303

304 ROI definition and analysis

305 Five regions of interest (ROIs) were defined in standard MNI space (see table 2). Contrasts
306 analysed for each ROI were 1) route vs. scrambled, 2) echo vs. no-echo, and 3) sound vs.
307 silence. FSL's Featquery was used to extract percent signal change (PSC) associated with each
308 of the three contrasts for each ROI for each participant.

309

310 <Table 2>

311

312 Whole Brain Analysis

313 In addition to the ROI analysis, we also ran a series of whole-brain analyses. First, we ran a
314 between-subject ANOVA to identify brain areas in which there was a significant difference
315 between the three groups (i.e. testing whether EE = BC = SC) for each stimulus contrast.
316 Following this, we calculated averages for each group (i.e. one-sample t tests) for each
317 contrast (same as those used in the ROI analysis). Z statistic images (Gaussianised T/F) were
318 thresholded using cluster-based thresholding determined by $Z > 2.3$ and a cluster significance
319 threshold of $p = 0.05$ (corrected using Gaussian Random Field theory; Worsley 2001).

320

321 In order to objectively assign anatomical labels to activation clusters, the coordinates of the
322 peak activity within each cluster were extracted, along with the coordinates of the local
323 maxima within each cluster, and these was used to extract corresponding labels from the
324 Jülich Histological Cyto-Architectonic Atlas (Eickhoff *et al.*, 2007) and MNI structural atlas

325 (Collins *et al*, 1995; Mazziotta *et al*, 2001). Where the atlases returned probabilistic values of
326 at least 25% for a particular anatomical label, this label was then assigned to that cluster.

327

328 Results

329 Behavioural

330 For the data collected prior to MR scanning, we calculated the proportion of correct
331 responses for three different measures of performance: specific route identification, route
332 vs. scrambled identification, and echo identification. One-way ANOVAs (with subject group
333 as the between-subject variable) were used to test for group differences for each of these
334 measures in performance, reported below (in addition to non-parametric Kruskal-Wallis
335 tests). Behavioural performance during fMRI was also analysed in the same way, and the
336 pattern of results was consistent with what we observed prior to scanning. We found the in-
337 scanner measure to be more variable, however, due to participants pressing more than one
338 key accidentally or failing to respond on some trials.

339

340 Specific route identification

341 When considering specific route identification, a response was correct when participants
342 identified the specific route (single-turn; two-turns-same; two-turns-different) when it was
343 presented. Thus, specific route identification measures participants' ability to correctly
344 identify specific echo-acoustic routes. There was a significant group difference in route
345 identification ($F(2,29) = 26.159$, $p < .001$, $\eta^2 = 0.643$; Kruskal-Wallis: $H(2)=13.830$, $p<.001$).
346 EEs (mean = .806) were significantly more accurate than BCs (mean = .475; $p < .001$; and
347 $p<.001$ with BC6 excluded) and SCs (mean = .470; $p < .001$). BCs and SCs were not
348 significantly different to one another ($p = 1.000$). These data are shown in figure 2a.

349

350 Route vs. scrambled identification

351 When considering scrambled vs. route identification, a response was identified as correct
352 when participants gave a 'scrambled' response to a scrambled sound, but also when they
353 gave any of the route responses when any of the route sounds were presented (regardless of
354 whether it was a single turn, two-turn-same or two-turn-different). Thus, scrambled vs. route
355 identification measures participants' ability to distinguish spatially coherent echo-acoustic
356 sounds from spatially incoherent echo-acoustic sounds. There was a significant group
357 difference in this measure ($F(2,29) = 10.681, p < .001, \eta^2 = 0.424$; Kruskal-Wallis:
358 $H(2)=13.719, p<.001$). EEs (mean = .962) were significantly more accurate than BCs (mean =
359 .790; $p = .001$; and $p=.002$ with BC6 excluded) and SCs (mean = .784; $p < .001$). BCs and SCs
360 were not significantly different to one another ($p = 1.000$). These data are shown in figure
361 2b.

362

363

364 Echo vs. no-echo identification

365 When considering echo identification, a response was identified as correct when participants
366 responded with 'no echo' when stimuli containing no echoes were present, and also when
367 participants gave any other response when any of the other stimuli were presented (e.g. if a
368 'single turn' route was labelled as 'scrambled', then this would be classed as correct because
369 the sound contains echoes). Thus, echo identification measures participants' ability to
370 distinguish echo from non-echo sounds. There was no significant group difference in this
371 measure ($F(2,29) = 2.507, p = .099$; Kruskal-Wallis: $H(2)=3.710, p=.156$). This is likely because
372 all groups had very high accuracy (EEs mean = 1.000; BCs mean = .963; SCs mean = .986).

373 This high level of performance in detecting the presence of echoes even for naïve
374 echolocators is consistent with our previously published results (Norman & Thaler, 2020;
375 2021). These data are shown in figure 2c.

376

377 Overall, these results suggest that EEs as a group performed better than both BCs and SCs for
378 those measures where spatial interpretation of echo information was required (i.e. route vs.
379 scrambled and route identification), but not for simple echo detection. Also, BCs and SCs did
380 not perform different from one another on any measure, suggesting that experience with
381 echolocation rather than blindness drives performance in this task.

382

383 <Figure 2>

384

385

386 fMRI – ROI analysis

387 The group means for all contrasts are shown in figure 3 (the individual data for the six EEs are
388 shown in table 3). We tested for group differences in PSC for each ROI and for each contrast
389 using one-way ANOVAs (subject group as the between-subject variable) and non-parametric
390 Kruskal-Wallis tests. Each resulting p value was Bonferroni-corrected by multiplying it by 5
391 (the number of ROIs). Any results in which these corrected p values were less than .05 are
392 reported as significant (thus, the alpha level was effectively .0083). Post-hoc tests were also
393 Bonferroni-corrected by a factor of 3 (the number of multiple comparisons). One-sample t
394 tests and non-parametric Wilcoxon signed-rank tests were also used to test whether PSC in
395 each ROI was significantly different from zero. The issue of multiple comparisons was
396 addressed using the Benjamini-Hochberg method to control false discovery rate (FDR, set at

397 .05; Benjamini & Hochberg, 1995). This was chosen over the highly conservative Bonferroni
398 adjustment due to the large number of tests (15 for each contrast). Briefly, this method
399 involves ranking the observed p values in order of size and calculating a Benjamini-Hochberg
400 critical value for each one (based on the rank number and the FDR). Any p values that are
401 less than the critical value for their rank are considered to be statistically significant. Thus,
402 the p values reported for these tests are not adjusted *per se*, but results are only reported as
403 significant where the p values were less than the Benjamini-Hochberg critical value.

404

405

406 <Figure 3>

407 <Table 3>

408

409 Route vs. scrambled

410 For the route vs. scrambled contrast, a significant group difference was found in the OPA
411 $F(2,29) = 13.344, p < .001, \eta^2 = .479$; Kruskal-Wallis: $H(2)=12.370, p=.010$). The EE group
412 showed significantly greater PSC than the BC ($p = .001$; and $p=.002$ with BC6 excluded) and SC
413 ($p < 0.001$) groups. The BC and SC groups did not differ ($p = .732$; and $p=.657$ with BC6
414 excluded). None of the other ROIs showed a significant difference between groups (A1:
415 $F(2,29) = .266, p = 1.000$; Kruskal-Wallis: $H(2)=.401, p=1.000$; V1: $F(2,29) = .563, p = 1.000$;
416 Kruskal-Wallis: $H(2)=1.167, p=1.000$; PHPA: $F(2,29) = .636, p = 1.000$; Kruskal-Wallis:
417 $H(2)=1.289, p=1.000$; SPL: $F(2,29) = 1.405, p=1.000$; Kruskal-Wallis: $H(2)=1.791, p=1.000$).

418

419 PSC in the OPA was significantly greater than zero for the EE group ($t(5) = 5.591, p = .003$;
420 Wilcoxon signed rank: $z = 2.201, p = .028$). No other tests showed a significant difference from
421 zero.

422

423 Our SCs were, on average, younger than our EEs. To test the possibility that age might be a
424 determining factor in the strength of response in the OPA, we correlated age with the route
425 vs. scrambled response in the OPA in our SC groups and found no significant association
426 ($r(12) = .316, p = .272$).

427

428

429 Echo vs. no-echo

430 A significant group difference was found in V1 ($F(2,29) = 14.837, p < .001, \eta^2 = .506$; Kruskal-
431 Wallis: $H(2) = 13.479, p = .006$). The EE group showed significantly greater PSC than the BC ($p <$
432 $.001$; and $p = .001$ with BC6 excluded) and SC ($p < .001$) groups. The BC and SC groups did
433 not differ ($p = .824$). A significant group difference was also found in the OPA ($F(2,29) =$
434 $14.979, p < .001, \eta^2 = .508$; Kruskal-Wallis: $H(2) = 14.779, p = .003$). The EE group showed
435 significantly greater PSC than the BC ($p = .005$; and $p = .005$ with BC6 excluded) and SC ($p <$
436 $.001$) groups. The BC and SC groups did not differ ($p = 0.072$). None of the other ROIs
437 showed a significant group effect (A1: $F(2,29) = 2.443, p = .523$; Kruskal-Wallis: $H(2) = 5.643,$
438 $p = .298$; PHPA: $F(2,29) = 4.818, p = .078$; Kruskal-Wallis: $H(2) = 11.388, p = .017$; SPL: $F(2,29) =$
439 $1.618, p = 1.000$; Kruskal-Wallis: $H(2) = 3.632, p = .814$).

440

441 PSC in V1 was significantly greater than zero for the EE group ($t(5) = 4.628, p = .006$; Wilcoxon
442 signed rank: $z = 2.201, p = .028$). PSC in A1 was significantly greater than zero for the SC group

443 (t(13) = 5.641, $p < .001$; Wilcoxon signed rank: $z = 3.233$, $p = .001$). PSC in PHPA was
444 significantly lower than zero for the SC group (t(13) = 5.282, $p < .001$; Wilcoxon signed rank:
445 $z = 2.982$, $p = .003$). No other tests showed a significant difference from zero.

446

447 Sound vs. silence

448 A significant group difference was found in V1 ($F(2,29) = 5.872$, $p = .036$, $\eta^2 = .288$; but note
449 Kruskal-Wallis was not significant: $H(2) = 8.228$, $p = .082$). The EE group showed significantly
450 greater PSC than the SC group ($p = .006$) but not the BC group ($p = .050$; and $p = .086$ with
451 BC6 excluded). The BC and SC groups did not differ ($p = .180$). A significant group difference
452 was also found in the OPA ($F(2,29) = 9.965$, $p = .003$, $\eta^2 = .407$; Kruskal-Wallis: $H(2) = 11.366$,
453 $p = .017$). The EE group showed significantly greater PSC than the SC group ($p < .001$) but not
454 the BC group ($p = .069$; but $p = .018$ with BC6 excluded). The BC and SC groups did not differ
455 ($p = .071$). None of the other ROIs showed a significant group effect (A1: $F(2,29) = 2.337$, $p =$
456 $.573$; Kruskal-Wallis: $H(2) = 5.030$, $p = .404$; PHPA: $F(2,29) = 1.224$, $p = 1.000$; Kruskal-Wallis:
457 $H(2) = 3.331$, $p = .945$; SPL: $F(2,29) = .801$, $p = 1.000$; Kruskal-Wallis: $H(2) = 1.152$, $p = 1.000$).

458

459 PSC in A1 was significantly greater than zero for the SC group (t(13) = 9.313, $p < .001$;
460 Wilcoxon signed rank: $z = 3.296$, $p < .001$), BC group (t(11) = 3.174, $p = .009$; Wilcoxon signed
461 rank: $z = 2.197$, $p = .028$), and EE group (t(5) = 4.626, $p = .006$; Wilcoxon signed rank: $z = 2.201$,
462 $p = .028$). PSC in V1 was significantly greater than zero for the EE group (t(5) = 4.394, $p = .007$;
463 Wilcoxon signed rank: $z = 2.201$, $p = .028$). PSC in PHPA was significantly lower than zero for
464 the SC group (t(13) = 3.631, $p = .003$; Wilcoxon signed rank: $z = 2.794$, $p = .005$). PSC in the
465 OPA was significantly greater than zero for the EE group (t(5) = 3.495, $p = .017$; Wilcoxon
466 signed rank: $z = 2.201$, $p = .028$). No other tests showed a significant difference from zero.

467

468 Additional ROI analyses: OPA activity and echolocation ability

469 It is possible that the activity observed in the OPA is only driven by high performance on the

470 route vs. scrambled identification task, regardless of participants being EEs, BCs or SCs. In our

471 study, BC and SC groups were, expectedly, less accurate on this task than the EE group. Thus,

472 to address the possibility that OPA activity in EEs is due to their more accurate task

473 performance, we ran two further analyses. First, we reran the route vs. scrambled contrast

474 analysis only using trials in which participants had classified correctly. To avoid differences in

475 statistical power between EEs and controls, we subsampled data from EEs to match number

476 of trials across groups. Analysing PSC in the OPA using only correct trials showed the same

477 pattern of results as we found when using all trials (EEs mean = .26, BCs mean = .10, SCs mean

478 = -.02) and there was a significant difference between groups ($F(2,29)=9.562$, $p=.003$,479 $\eta^2=.397$; Kruskal-Wallis: $H(2)=12.948$, $p=.008$), with EEs showing a significantly greater480 response compared to SCs ($p<.001$) but not BCs ($p=.067$). BCs and SCs were not significantly481 different to one another ($p=.090$). Applying the Benjamini-Hochberg method, only the EE482 group showed a response in the OPA significantly greater than zero ($t(5)=5.604$, $p=.003$;483 Wilcoxon signed rank: $z= 2.201$, $p=.028$). Secondly, to further investigate possible

484 associations between behavioural performance and OPA response (for the route vs.

485 scrambled contrast), we ran a correlation analysis which revealed for EEs a borderline

486 significant correlation between behavioural performance and PSC in the OPA ($r(4)=.808$,487 $p=.052$), but no correlation for BCs ($r(10)=.361$, $p=.249$) or SCs ($r(12)=-.001$, $p=.998$). Figure 4

488 shows the scatter plot of these data. These results suggest that responses in the OPA are not

489 driven solely by the ability to identify route vs. scrambled sounds, but is likely the result of

490 both long-term echolocation experience and task-specific echolocation ability.

491

492 <Figure 4>

493

494

495

496 Additional ROI analyses: functionally localised OPA ROI

497 In the sighted brain, the location of the OPA is typically defined using a functional localiser

498 with the contrast of static visual scenes > static visual objects (e.g. Sun *et al*, 2021; Kamps *et*499 *al*, 2016; Dilks *et al*, 2013). In our study, this region was defined as a single sphere centred on

500 the average MNI coordinates from an independent study that used the functional localiser in

501 17 sighted subjects (Sun *et al*, 2021). To verify that our observed activation in the OPA EEs

502 corresponds to the functionally defined OPA, we carried out an additional analysis using

503 localiser data for 14 sighted adults from a second independent study (Meissner *et al*, 2019).504 The raw data were obtained through Open Science Framework (<https://osf.io/aydqz/>) and

505 analysed using FSL's FEAT pre-processing (brain-extraction, non-linear registration at 2-mm

506 resolution, slice-timing correction, motion correction, high-pass temporal filtering at 70 s,

507 and spatial smoothing at 5 mm) and mixed effects statistical model. The group-level

508 statistical map for the contrast scenes > objects was thresholded using clusters determined

509 by $Z > 4.00$ and a (corrected) cluster significance threshold of $p = .05$, and we used this result to

510 identify two clusters in occipital cortex that were centred at approximately spatially mirrored

511 locations across the left and right hemispheres (left: -36, -74, 26, number of voxels = 153;

512 right: 34, -78, 20, number of voxels = 166). The coordinates of those clusters corresponded

513 well to those from Sun *et al* (2021; left: -29.4, -83.8, 23.9; right: 35.7, -78.5, 23.7). We then

514 used these cluster masks as ROIs with which to analyse PSC for the route vs. scrambled

515 contrast. Replicating our original finding, EEs showed a significant response for route vs.
516 scrambled in left ($t(5)=3.930$, $p=.011$; Wilcoxon signed rank $z= 2.201$, $p=.028$) and right
517 hemisphere ROIs ($t(5)=5.074$, $p=.004$; Wilcoxon signed rank $z= 2.201$, $p=.028$).

518

519 Additional ROI analyses – PSC for individual stimulus conditions

520 Furthermore, in order to determine the nature of the effect(s) underlying the response in the
521 OPA in EEs, we analysed the PSC in this area in response to each of the three individual
522 stimulus conditions (i.e. relative to silence baseline) and compared these to the same values
523 in control regions A1 and V1. These values (and those for all ROIs) are shown in figure 5. In a
524 two-way within-subject ANOVA with the factors ROI (OPA, A1, V1) and stimulus (route,
525 scrambled, no echo), there was a significant interaction ($F(4,20)=5.446$, $p=.004$, $\eta_p^2 = .521$).
526 This implies a difference in response profiles across the three ROIs to the different stimuli.
527 This was further explored in separate ANOVAs for each ROI. In the OPA there was a
528 significant difference between stimulus conditions ($F(2,10)=11.457$, $p=.003$, $\eta_p^2 = .696$), with
529 route sounds evoking greater PSC compared to no echo sounds ($t(5)=3.674$, $p=.014$) and
530 scrambled sounds ($t(5)=5.613$, $p=.002$). Scrambled sounds did not evoke significantly
531 stronger PSC compared to no echo sounds ($t(5)=2.479$, $p=.056$). In contrast, in A1 there was
532 no significant difference between stimulus conditions ($F(2,10)=.371$, $p=.699$). In V1, there
533 was a significant difference ($F(2, 10)=14.725$, $p=.001$, $\eta_p^2 = .747$), with route sounds evoking
534 greater PSC compared to no echo sounds ($t(5)=4.907$, $p=.004$) but not scrambled sounds
535 ($t(5)=1.054$, $p=.340$), although scrambled sounds did evoke greater PSC compared to no echo
536 sounds ($t(5)=3.727$, $p=.014$). Furthermore, by considering PSC to the individual stimulus
537 conditions, we were able to validate using one-sample t tests (applying the Benjamini-
538 Hochberg method, as previously described) that in OPA route sounds evoked activity

539 significantly greater than zero ($t(5) = 3.988$, $p = .010$; Wilcoxon signed rank $z = 2.201$, $p = .028$),
540 whilst neither scrambled ($t(5) = 2.889$, $p = .034$; note that this is a non-significant result when
541 p value is compared against the Benjamini-Hochberg critical value of $.023$; Wilcoxon signed
542 rank $z = 2.201$, $p = .028$) nor no-echo sounds ($t(5) = .685$, $p = .524$; Wilcoxon signed rank $z = .524$,
543 $p = .600$) led to significant activity. All significant one-sample t -tests are displayed on figure 5.

544

545 <Figure 5>

546

547 For BCs, the same analysis did not reveal a significant interaction between stimulus condition
548 and ROI ($F(4,44) = .729$, $p = .577$). For SCs, there was a significant interaction ($F(4,52) = 11.003$,
549 $p < .001$, $\eta_p^2 = .458$). Further ANOVAs revealed that in the OPA there was a significant
550 difference between stimulus conditions ($F(2,10) = 3.468$, $p = .046$, $\eta_p^2 = .211$), with route
551 sounds evoking *less* PSC compared to no echo sounds ($t(5) = 2.194$, $p = .047$). There was no
552 difference between scrambled sounds and route sounds ($t(5) = .693$, $p = .500$) or between
553 scrambled sounds and no echo sounds ($t(5) = 1.881$, $p = .083$). In A1 there was also significant
554 difference between conditions ($F(2,26) = 24.034$, $p < .001$, $\eta_p^2 = .649$), which was driven by click
555 sounds evoking less PSC compared to both scrambled ($t(13) = 5.109$, $p < .001$) and route sounds
556 ($t(13) = 5.572$, $p < .001$), but no difference between scrambled and route sounds ($t(13) = 1.273$,
557 $p = .225$). There was no significant difference between stimulus conditions in V1 ($F(2,$
558 $26) = .344$, $p = .712$). Neither BCs nor SCs showed significant PSC in the OPA in response to any
559 of the stimulus conditions.

560 Overall, these results show that the OPA in EEs has a unique response profile across the three
561 stimulus conditions compared to the other ROIs and to the other control groups. This
562 response profile is consistent with its role in processing spatially coherent echo-acoustic
563 sounds for navigation.

564

565

566 fMRI – whole-brain analysis

567

568 Route vs. scrambled

569 Results for the analysis of a group difference for the route vs. scrambled contrast on the
570 whole brain are shown in figure 6. These results reveal significant clusters in and around the
571 OPA ROI and other occipital and parietal regions. Separate whole-brain activation maps for
572 each subject group are shown in figure 7. For this contrast, EEs showed two activation
573 clusters. The largest was centred on the superior parietal lobule (subregion 7P) in the left
574 hemisphere, and the other was centred on the inferior parietal lobule (subregion PGp) in the
575 right hemisphere. Both of these clusters extend into the OPA region, and are therefore
576 consistent with the findings from our ROI analysis. BCs did not show any significant clusters.
577 SCs, however, did show four significant clusters. Three of these covered similar areas
578 identified in EEs (i.e. superior/inferior parietal lobules), in addition to anterior parietal sulcus
579 and some frontal areas (motor cortex and Broca's area). None of the activation clusters for
580 SCs extended into the OPA region. A detailed summary of the activation clusters found for
581 the route vs. scrambled contrast is shown in table 4.

582

583 <Figure 6>

584 <Figure 7>

585 <Table 4>

586

587 We also quantified the degree of spatial overlap between the cluster maps for the EEs' route
588 vs. scrambled contrast and the functionally defined OPA ROI resulting from the analysis of
589 Meissner *et al's* (2019) sighted localiser data (see section 'Additional ROI analyses:
590 functionally localised OPA ROI' for cluster description). In the right hemisphere, the spatial
591 overlap covered 77 voxels (46% of all voxels in the sighted localiser cluster and 25% EEs'
592 route vs. scrambled cluster). In the left hemisphere the spatial overlap covered 32 voxels
593 (21% of voxels in the sighted localizer cluster, and 4%, in EE's route vs. scrambled cluster).
594 The low percentage of overlap in EEs in the left hemisphere is attributable to the fact that
595 this cluster in EEs is comparably larger, extending further into the parietal lobe (compare
596 table 4 and figure 7).

597

598 Echo vs. no-echo

599 Results for the analysis of a group difference for the echo vs. no echo contrast on the whole
600 brain are shown in figure 8. These results reveal large areas of activation in occipital and
601 parietal cortex. Separate whole-brain activation maps for each subject group are shown in
602 figure 9. The pattern of results was similar across BCs and SCs and included primary auditory
603 cortex, premotor cortex, and parietal areas (anterior intraparietal sulcus and superior/inferior
604 parietal lobules). There were also significant activation clusters in Broca's areas in both
605 groups. The pattern of activity observed for the EE group included similar areas that were
606 activated in the BC and SC groups, but additionally included a large activation cluster in early
607 visual cortex. Detailed descriptions of these clusters are shown in table 5.

608

609 <Figure 8>

610 <Figure 9>

611 <Table 5>

612

613 Sound vs. Silence

614 Results for the analysis of a group difference for the sound vs. silence contrast on the whole
615 brain are shown in figure 10. These results reveal similar areas of activation to the echo vs.
616 no echo contrast. Separate whole-brain activation maps for each subject group are shown
617 in figure 11. All three groups showed significant activation clusters in a number of different
618 brain areas (this is to be expected, based on the non-specific nature of the contrast). Most
619 notably, these activation clusters included primary auditory cortex, motor/premotor cortex,
620 and parietal areas (anterior parietal sulcus and superior/inferior parietal lobules). The EE
621 group was the only group that also showed a significant activation cluster in early visual
622 cortex. Detailed descriptions of these clusters are shown in table 6.

623

624 <Figure 10>

625 <Figure 11>

626 <Table 6>

627

628

629

630 Discussion

631 In the present study, we have shown that the occipital place area (OPA) is recruited in blind
632 echolocation experts (EEs) during traversal of a virtual echo-acoustic space in first-person
633 perspective. This was not found in blind or sighted controls (BCs or SCs, respectively). The
634 task we used can be considered an echo-acoustic analogue of a vision-based task that has
635 previously been found to evoke activation in the OPA in sighted people (Kamps *et al*, 2016).
636 Our study, therefore, provides evidence that the OPA is not uniquely associated with visually
637 guided navigation, but can also be similarly recruited for echo-acoustic navigation. ROI and
638 whole-brain analyses provided converging evidence for OPA involvement, and our
639 behavioural measures verified that EEs could discriminate coherent route sounds from
640 scrambled sounds. Further, the critical contrast was based on sounds that controlled for
641 spectro-temporal acoustic properties.

642

643 The OPA has been previously identified as an important part of the human navigation brain
644 network, being associated with visual perception of static scenes (Dilks *et al*, 2013) as well as
645 dynamic boundary-based spatial navigation (Kamps *et al*, 2016; Julian *et al*, 2016). Julian and
646 colleagues (2016), for example, used TMS to show that, in sighted people, the OPA is causally
647 involved in the encoding of object locations relative to boundaries in the environment.
648 Specifically, they hypothesise that the OPA serves as the source of the perceptual
649 representation of environmental boundary information, which is then used in the spatial
650 coding of the environment in the larger network of navigation-related brain regions. It is also
651 known that the OPA and PHPA are functionally connected (Baldassano *et al*, 2013), which
652 might mediate input from the OPA to the hippocampal formation (Naber *et al*, 1997). What
653 the present study demonstrates, however, is that the perceptual representation formed in

654 the OPA is not necessarily formed through visual input, and can also be formed in the
655 absence of vision.

656

657 Participants in the BC but not EE group tended to have some residual visual sensitivity. It is
658 thus possible that complete blindness itself, rather than echolocation experience, is sufficient
659 to elicit OPA responses to echo-acoustic sounds. In this context it is important to note that
660 our BCs and SCs were very similar in their brain activations, whilst both groups differed
661 greatly from EEs. This suggests that long term experience in echolocation rather than
662 blindness *per se* underlies the response in the OPA. Furthermore, our additional analyses
663 also suggested that the activity in the OPA was unique to EEs and not simply driven by
664 participants' accuracy at identifying route vs. scrambled sounds, regardless of them being
665 EEs, BCs or SCs. Specifically, our data suggested that, although OPA activity was significantly
666 higher for EEs compared to the control groups, there was no evidence in the control groups
667 that this activity was predicted by their task performance. In contrast, the pattern of results
668 *within* the six EEs indicated a positive association (though only borderline statistically
669 significant) between task performance and OPA activity. This dual influence of long-term
670 echolocation experience and task specific ability is strikingly similar to our previous finding
671 that both long-term echolocation experience *and* echo-localisation acuity predict the degree
672 of retinotopic-like mapping of sounds in V1 (Norman *et al*, 2019).

673

674 With respect to activations in parietal cortices (in particular SPL), our ROI analysis, which
675 considered SPL as combination of subareas 5Ci, 5L, 5M, 7A, 7M, 7P, did not show any
676 significant involvement for any contrast or participant group. Yet, the whole brain analysis

677 revealed significant clusters of activation for subareas of SPL for different participant groups
678 and contrasts. These activations are generally consistent with those reported in a previous
679 study examining echolocation-based route following (Fiehler *et al*, 2015). The result by
680 Fiehler *et al* (2015), however, was based on the contrast echo vs. no-echo sounds, but the
681 present results from our route vs. scrambled contrast do suggest that the activation in SPL
682 reflects the processing of the coherent spatiotemporal structure of echolocation navigation
683 sounds. The SPL has also been shown to be active in sighted people whilst solving a vision-
684 based route recognition task, and in blind people solving the same task using a sensory
685 substitution device (Kupers *et al*, 2010). The specific functional role that the SPL might play
686 in navigation remains unclear, but it has previously been associated with the egocentric
687 coding of visual space (Galati *et al*, 2000).

688

689 In addition to SPL, both EEs and SCs showed activation in the inferior parietal lobule (area
690 PGp), with SCs showing additional activation in the anterior intra-parietal sulcus (aIPS).
691 Fiehler *et al* (2015) also found some activation in these areas in SCs, and the aIPS has also
692 previously been associated with egocentric spatial coding (Galati *et al*, 2000). A recent study
693 found activation within the visual dorsal stream (i.e. parietal cortex), including a posterior
694 area close to the occipitoparietal sulcus (V6/V6a complex), in both blind and sighted
695 blindfolded participants when using a visual-to-auditory SSD to navigate a virtual
696 environment (after training; Maidenbaum *et al*, 2018). Together with our results, these
697 findings suggest that there are several areas within parietal cortex that might play a role in
698 navigation (with or without vision). It is important to note, however, that areas of posterior
699 parietal cortex such as aIPS and SPL are more generally also considered to be part of the

700 dorsal frontoparietal attention network (Szczepanski, Pinsk, Douglas, Kastner & Saalman,
701 2013) – a network that is thought to control top-down attention to environmental objects
702 and tasks (Corbetta *et al*, 2008; Corbetta & Schulman, 2002). Although this network is
703 typically described with respect to visual processing, effects of spatial attention within the
704 auditory modality have also been observed in posterior parietal cortex (Shomstein & Yantis,
705 2006). Thus, it remains unclear whether the activity in these posterior parietal areas reflects
706 processes specific to navigation, the multimodal perception of space, or the effects of spatial
707 attention. It is, of course, possible that these areas contribute to complex tasks such as the
708 one used here in a number of ways.

709

710 We found no evidence of positive activity in the parahippocampal place area for the contrast
711 route vs. scrambled. The parahippocampal place area is considered to be central to the
712 spatial navigation network in humans (i.e. parahippocampal cortex; Hartley *et al*, 2003;
713 2014). The absence of activity in our paradigm is consistent with studies using a similar
714 paradigm to ours (e.g. Fiehler *et al*, 2015; Kamps *et al*, 2016) and is likely the result of the
715 nature of the task requirements. Specifically, participants were not required to navigate
716 previously learned environments or to match routes to those held in memory, but were
717 instead required to identify the directions of the turns taken along each route. This task
718 design was chosen so we could include a suitable control condition (scrambled sounds) to
719 rule out activity driven by spectro-temporal properties of the stimuli. Kupers and colleagues
720 (2010), in contrast, required participants using a visual-to-tactile SSD to explicitly match one
721 of two sample routes to a previous one and found parahippocampal activity in blind
722 participants. Interestingly, for our echo vs. no-echo and sound vs. silence contrasts we found
723 evidence of negative activity in the parahippocampal place area in SCs. This is similar to the

724 findings of Maidenbaum and colleagues (2018), in which negative activity in the medial
725 temporal lobe was found in blind and sighted participants when navigating using a visual-to-
726 auditory SSD. The implication of this negative activity remains unclear.

727

728 Both ROI and whole brain analysis showed activation in occipital cortex, including early visual
729 cortex, in the EE group for the contrast echo vs. no-echo. This activation was in addition to
730 activity in other areas, including parietal areas, and Broca's areas, which was present in all
731 three groups. The same pattern of results was also observed for the sound vs. silence
732 contrast, for which additional activity was also observed in all three groups' primary auditory
733 areas. This pattern of results strongly suggests that recruitment of V1 for processing of echo-
734 acoustic information is tied to experience with echolocation rather than blindness *per se*. It is
735 by now well-established that the neural correlates of echolocation in EEs include several
736 areas of occipital cortex typically associated with inherently visual functions, including V1
737 (Arnott *et al*, 2013; Fiehler *et al*, 2015; Flanagan *et al*., 2016; Norman & Thaler, 2019; Milne *et*
738 *al*, 2015; Thaler *et al*, 2011; Thaler *et al*, 2014; Wallmeier *et al*., 2015). The results of the
739 present study therefore lend further support to the notion that the organization of the
740 human brain is not strictly tied to specific modalities, but organised flexibly according to task
741 demands, and shaped by experience with a specific task or computation (e.g. echolocation),
742 rather than sensory experience *per se* (e.g. blindness; see Amedi *et al*, 2017).

743

744 In conclusion, the present study found that the OPA – an area previously assumed to be
745 strongly associated with boundary-based visually-guided navigation – is driven in EEs during
746 echo-acoustically guided navigation. This opens up novel ways of understanding the brain
747 areas and networks typically involved in visual spatial navigation.

748 References

- 749 Amedi, A., Hofstetter, S., Maidenbaum, S., & Heimler, B. (2017). Task selectivity as a comprehensive
750 principle for brain organization. *Trends in cognitive sciences*, 21(5), 307-310.
- 751 Andersson J. L. R., Jenkinson, M., Smith, S. (2010) Non-linear registration, aka spatial
752 normalisation. [FMRIB technical report TR07JA2](#)
- 753 Arnott, S. R., Thaler, L., Milne, J. L., Kish, D., & Goodale, M. A. (2013). Shape-specific activation of
754 occipital cortex in an early blind echolocation expert. *Neuropsychologia*, 51(5), 938-949.
- 755 Baldassano, C., Beck, D. M., & Fei-Fei, L. (2013). Differential connectivity within the parahippocampal
756 place area. *Neuroimage*, 75, 228-237.
- 757 Beckmann, C. F., Jenkinson, M., & Smith, S. M. (2003). General multilevel linear modeling for group
758 analysis in FMRI. *Neuroimage*, 20(2), 1052-1063.
- 759 Benjamini, Y., & Hochberg, Y. (1995). Controlling the false discovery rate: a practical and powerful
760 approach to multiple testing. *Journal of the Royal statistical society: series B (Methodological)*, 57(1),
761 289-300.
- 762 Boccia, M., Nemmi, F., & Guariglia, C. (2014). Neuropsychology of environmental navigation in
763 humans: review and meta-analysis of FMRI studies in healthy participants. *Neuropsychology*
764 *review*, 24(2), 236-251.
- 765 Brainard, D. H. (1997). The psychophysics toolbox. *Spatial vision*, 10(4), 433-436.
- 766 Chan, E., Baumann, O., Bellgrove, M. A., & Mattingley, J. B. (2012). From objects to landmarks: the
767 function of visual location information in spatial navigation. *Frontiers in psychology*, 3, 304.
- 768 Collins, D. L., Holmes, C. J., Peters, T. M., & Evans, A. C. (1995). Automatic 3-D model-based
769 neuroanatomical segmentation. *Human brain mapping*, 3(3), 190-208.
- 770 Corbetta, M., Patel, G., & Shulman, G. L. (2008). The reorienting system of the human brain: from
771 environment to theory of mind. *Neuron*, 58(3), 306-324.
- 772 Corbetta, M., & Shulman, G. L. (2002). Control of goal-directed and stimulus-driven attention in the
773 brain. *Nature reviews neuroscience*, 3(3), 201-215.

- 774 Dilks, D. D., Julian, J. B., Paunov, A. M., & Kanwisher, N. (2013). The occipital place area is causally
775 and selectively involved in scene perception. *Journal of Neuroscience*, 33(4), 1331-1336.
- 776 Dodsworth, C., Norman, L. J., & Thaler, L. (2020). Navigation and perception of spatial layout in
777 virtual echo-acoustic space. *Cognition*, 197, 104185.
- 778 Eickhoff, S. B., Paus, T., Caspers, S., Grosbras, M. H., Evans, A. C., Zilles, K., & Amunts, K. (2007).
779 Assignment of functional activations to probabilistic cytoarchitectonic areas
780 revisited. *Neuroimage*, 36(3), 511-521.
- 781 Ekstrom, A. D. (2015). Why vision is important to how we navigate. *Hippocampus*, 25(6), 731-735.
- 782 Ekstrom, A. D., Huffman, D. J., & Starrett, M. (2017). Interacting networks of brain regions underlie
783 human spatial navigation: a review and novel synthesis of the literature. *Journal of Neurophysiology*,
784 118 (6), 3328-3344.
- 785 Epstein, R., Harris, A., Stanley, D., & Kanwisher, N. (1999). The parahippocampal place area:
786 recognition, navigation, or encoding?. *Neuron*, 23(1), 115-125.
- 787 Fiehler, K., Schütz, I., Meller, T., & Thaler, L. (2015). Neural correlates of human echolocation of path
788 direction during walking. *Multisensory research*, 28(1-2), 195-226.
- 789 Flanagan, V. L., Schörnich, S., Schranner, M., Hummel, N., Wallmeier, L., Wahlberg, M., Stephan, T.
790 & Wiegrebe, L. (2017). Human exploration of enclosed spaces through echolocation. *Journal of*
791 *Neuroscience*, 37(6), 1614-1627.
- 792 Galati, G., Lobel, E., Vallar, G., Berthoz, A., Pizzamiglio, L., & Le Bihan, D. (2000). The neural basis
793 of egocentric and allocentric coding of space in humans: a functional magnetic resonance
794 study. *Experimental brain research*, 133(2), 156-164.
- 795 Griffin, D. R. (1944). Echolocation by blind men, bats and radar. *Science*, 100(2609), 589-590.
- 796 Hall, D. A., Haggard, M. P., Akeroyd, M. A., Palmer, A. R., Summerfield, A. Q., Elliott, M. R., ... &
797 Bowtell, R. W. (1999). "Sparse" temporal sampling in auditory fMRI. *Human brain mapping*, 7(3), 213-
798 223.
- 799 Hartley, T., Maguire, E. A., Spiers, H. J., & Burgess, N. (2003). The well-worn route and the path less
800 traveled: distinct neural bases of route following and wayfinding in humans. *Neuron*, 37 (5),

801 877-888.

802 Hartley, T., Lever, C., Burgess, N. and O'Keefe, J. (2014). Space in the brain: How the hippocampal
803 formation supports spatial cognition, *Philos. Trans. R. Soc. B Biol. Sci.* **369**(1635), 20120510.

804 DOI:10.1098/rstb.2012.0510.

805 Jenkinson, M., & Smith, S. (2001). A global optimisation method for robust affine registration of brain
806 images. *Medical image analysis*, *5*(2), 143-156.

807 Jenkinson, M., Bannister, P., Brady, M., & Smith, S. (2002). Improved optimization for the robust and
808 accurate linear registration and motion correction of brain images. *Neuroimage*, *17*(2), 825-841.

809 Julian, J. B., Ryan, J., Hamilton, R. H., & Epstein, R. A. (2016). The occipital place area is causally
810 involved in representing environmental boundaries during navigation. *Current Biology*, *26*(8), 1104-
811 1109.

812 Kamps, F. S., Lall, V., & Dilks, D. D. (2016). The occipital place area represents first-person
813 perspective motion information through scenes. *Cortex*, *83*, 17-26.

814 Kolarik, A. J., Cirstea, S., Pardhan, S., & Moore, B. C. (2014). A summary of research investigating
815 echolocation abilities of blind and sighted humans. *Hearing research*, *310*, 60-68.

816 Kong, X. Z., Wang, X., Pu, Y., Huang, L., Hao, X., Zhen, Z., & Liu, J. (2017). Human navigation
817 network: the intrinsic functional organization and behavioral relevance. *Brain Structure and*
818 *Function*, *222* (2), 749-764.

819 Kupers, R., Chebat, D. R., Madsen, K. H., Paulson, O. B. and Ptito, M. (2010). Neural correlates of
820 virtual route recognition in congenital blindness, *Proc. Natl Acad. Sci. USA* **107**, 12716–12721.

821 Loomis, J. M., Klatzky, R. L., & Golledge, R. G. (2001). Navigating without vision: basic and applied
822 research. *Optometry and vision science*, *78*(5), 282-289.

823 Maidenbaum, S., Chebat, D. R., & Amedi, A. (2018). Human navigation without and with vision-the
824 role of visual experience and visual regions. *BioRxiv*, 480558.

825 Mazziotta, J., Toga, A., Evans, A., Fox, P., Lancaster, J., Zilles, K., ... & Mazoyer, B. (2001). A
826 probabilistic atlas and reference system for the human brain: International Consortium for Brain

- 827 Mapping (ICBM). *Philosophical Transactions of the Royal Society of London. Series B: Biological*
828 *Sciences*, 356(1412), 1293-1322.
- 829 Meissner, T. W., Nordt, M., & Weigelt, S. (2019). Prolonged functional development of the
830 parahippocampal place area and occipital place area. *Neuroimage*, 191, 104-115.
- 831 Milne, J. L., Arnott, S. R., Kish, D., Goodale, M. A., & Thaler, L. (2015). Parahippocampal cortex is
832 involved in material processing via echoes in blind echolocation experts. *Vision research*, 109, 139-
833 148.
- 834 Naber, P. A., Caballero-Bleda, M., Jorritsma-Byham, B., & Witter, M. P. (1997). Parallel input to the
835 hippocampal memory system through peri-and postrhinal cortices. *Neuroreport*, 8(11), 2617-2621.
- 836 Norman, L. J., & Thaler, L. (2018). Human echolocation for target detection is more accurate with
837 emissions containing higher spectral frequencies, and this is explained by echo intensity. *i-*
838 *Perception*, 9(3), 2041669518776984.
- 839 Norman, L. J., & Thaler, L. (2019). Retinotopic-like maps of spatial sound in primary 'visual' cortex of
840 blind human echolocators. *Proceedings of the Royal Society B*, 286(1912), 20191910.
- 841 Norman, L. J., & Thaler, L. (2020). Stimulus uncertainty affects perception in human echolocation:
842 Timing, level, and spectrum. *Journal of Experimental Psychology: General*, 149(12), 2314.
- 843 Norman, L. J., & Thaler, L. (2021). Perceptual constancy with a novel sensory skill. *Journal of*
844 *Experimental Psychology: Human Perception and Performance*, 47(2), 269.
- 845 Shomstein, S., & Yantis, S. (2006). Parietal cortex mediates voluntary control of spatial and
846 nonspatial auditory attention. *Journal of Neuroscience*, 26(2), 435-439.
- 847 Smith, S. M. (2002). Fast robust automated brain extraction. *Human brain mapping*, 17(3), 143-155.
- 848 Sun, L., Frank, S. M., Epstein, R. A., & Peter, U. T. (2021). The parahippocampal place area and
849 hippocampus encode the spatial significance of landmark objects. *NeuroImage*, 236, 118081.
- 850 Szczepanski, S. M., Pinsk, M. A., Douglas, M. M., Kastner, S., & Saalmann, Y. B. (2013). Functional
851 and structural architecture of the human dorsal frontoparietal attention network. *Proceedings of the*
852 *National Academy of Sciences*, 110(39), 15806-15811.

- 853 Thaler, L. & De Vos, H.P.J.C. and Kish, D. and Antoniou, M. and Baker, C.J. and Hornikx,
854 M.C.J. (2019) 'Human click-based echolocation of distance: superfine acuity and dynamic clicking
855 behaviour.', *Journal of the Association for Research in Otolaryngology.*, 20 (5). pp. 499-510
- 856 Thaler, L., Arnott, S. R., & Goodale, M. A. (2011). Neural correlates of natural human echolocation in
857 early and late blind echolocation experts. *PLoS one*, 6(5), e20162.
- 858 Thaler, L., & Goodale, M. A. (2016). Echolocation in humans: an overview. *Wiley Interdisciplinary*
859 *Reviews: Cognitive Science*, 7(6), 382-393.
- 860 Thaler, L., Milne, J. L., Arnott, S. R., Kish, D., & Goodale, M. A. (2014). Neural correlates of motion
861 processing through echolocation, source hearing, and vision in blind echolocation experts and sighted
862 echolocation novices. *Journal of Neurophysiology*, 111(1), 112-127.
- 863 Thinus-Blanc, C., & Gaunet, F. (1997). Representation of space in blind persons: vision as a spatial
864 sense?. *Psychological bulletin*, 121(1), 20.
- 865 Wallmeier, L., Kish, D., Wiegrebe, L., & Flanagan, V. L. (2015). Aural localization of silent objects by
866 active human biosonar: Neural representations of virtual echo-acoustic space. *European Journal of*
867 *Neuroscience*, 41(5), 533-545.
- 868 Weiner, K. S., Barnett, M. A., Witthoft, N., Golarai, G., Stigliani, A., Kay, K. N., ... & Grill-Spector, K.
869 (2018). Defining the most probable location of the parahippocampal place area using cortex-based
870 alignment and cross-validation. *Neuroimage*, 170, 373-384.
- 871 Woolrich, M. W., Ripley, B. D., Brady, M., & Smith, S. M. (2001). Temporal autocorrelation in
872 univariate linear modeling of FMRI data. *Neuroimage*, 14(6), 1370-1386.
- 873 Woolrich, M. W., Behrens, T. E., Beckmann, C. F., Jenkinson, M., & Smith, S. M. (2004). Multilevel
874 linear modelling for FMRI group analysis using Bayesian inference. *Neuroimage*, 21(4), 1732-1747.
- 875 Woolrich, M. (2008). Robust group analysis using outlier inference. *Neuroimage*, 41(2), 286-301.
- 876 Worsley, K. J. (2001). Statistical analysis of activation images. *Functional MRI: An introduction to*
877 *methods*, 14(1), 251-70.
- 878
- 879

880 Tables

881

882 Table 1

883 Details of all blind participants, organised by group. EE refers to echolocation expert; BC

884 refers to blind control.

885

Participant	Sex	Age	Degree of vision loss	Cause and age of vision loss	Echolocation use
EE1	M	53	Total blindness	Enucleation due to retinoblastoma at 13 months.	Daily, since early childhood/no exact age remembered
EE2	M	60	Bright light detection both eyes	Retinal detachment; from birth	Daily, since age 6
EE3	M	49	Total blindness	Enucleation due to retinoblastoma at 18 and 30 months.	Daily, since 8 years old
EE4	M	24	Total blindness.	Vision loss suddenly at age 12 due to unknown causes. Enucleation at age 19 to alleviate ocular discomfort.	Daily, since 12 years old

EE5	M	37	Total blindness	Gradual sight loss since birth due to glaucoma.	Daily, since 12 years old
EE6	F	43	Total blindness.	Leber's congenital amaurosis, from birth	Daily, since 31 years old
BC1	F	60	Total blindness in left eye; some peripheral vision in right eye.	Stichler's syndrome. Retinal sciasis, from birth with increasing severity.	Some experience; very little regular use
BC2	M	38	Tunnel vision (<2 deg) and decreased acuity (< 20/200) in both eyes.	Retinitis Pigmentosa and other retinal pathology (unknown). Official diagnosis in early childhood (no exact age remembered but was known when commencing school, i.e. age 5yrs).	None
BC3	M	54	Residual bright light perception	Retinitis pigmentosa. Official diagnosis age 10 yrs. Gradual sight loss from birth.	Some experience; very little regular use
BC4	M	39	Residual bright light perception	Retinitis pigmentosa. Gradual sight loss from	None

				birth. Official diagnosis in early childhood (no exact age remembered but was known when commencing school, i.e. age 5yrs).	
BC5	F	44	Total Blindness right eye; bright light detection left eye.	Microphthalmia and Glaucoma; right eye enucleated aged 39 yrs	None
BC6	F	72	Bright Light detection.	Retinitis Pigmentosa. Gradual sight loss from birth. Official diagnosis in early childhood (no exact age remembered but was known when commencing school, i.e. age 5yrs).	None
BC7	M	46	Total blindness	Ocular albinism. Gradual sight loss from birth.	Some experience; very little regular use
BC8	F	36	Bright Light detection.	Unknown cause, from birth.	None
BC9	M	37	Tunnel vision (<5 deg) and decreased	Retinitis pigmentosa. Gradual sight loss from	None

			acuity (< 20/200) in both eyes.	birth. Official diagnosis age 13yrs.	
BC10	F	27	Left eye ca. 1 deg of foveal vision left with reduced acuity (<20/200); right eye bright light detection	Leber's Amaurosis and Cataracts, from birth.	None
BC11	F	79	Some blurred foveal vision; prone to bleaching	Rod Cone Dystrophy, from birth.	None
BC12	M	48	Total blindness in left eye; residual bright light perception in right eye.	Severe childhood glaucoma, from 3 months old.	None

886

887

888 **Table 2**

889 ROI details. For each named ROI, data were averaged across the left and right hemispheres

890 (unless stated otherwise). Where a probabilistic atlas was used to define the ROI, the

891 classification threshold is given (i.e. only voxels with a probabilistic value above this threshold

892 were included).

893

ROI label	Description
A1	Primary auditory cortex, based on areas TE 1.0, 1.1 and 1.2 in the Jülich histological (cyto- and myelo-architectonic) atlas (threshold > 50%).
V1	Primary visual cortex, based on area 17/V1 in the Jülich histological (cyto- and myelo-architectonic) atlas (threshold > 50%).
OPA	Sphere of 7.5-mm radius at approximate location of the occipital place area (OPA), based on average MNI coordinates (left: -29.4, -83.8, 23.9, right: 35.7, -78.5, 23.7) provided by Sun <i>et al</i> (2021). These coordinates were acquired using a scene > objects localiser, averaged across 17 participants.
PHPA	Parahippocampal place area (PHPA), based on probabilistic atlas from Weiner <i>et al</i> (2018), fitted to the MNI standard template.
SPL	Superior parietal lobule (SPL), based on the combination of subareas 5Ci, 5L, 5M, 7A, 7M, 7P, and 7PC in the Jülich histological (cyto- and myelo-architectonic) atlas (threshold > 50%).

894

895

896 **Table 3**

897 Individual PSC datapoints for the six EEs, organised by contrast and ROI (group means of
898 these data are shown in figure 3).

899

<i>Route vs scrambled</i>	A1	V1	PHPA	OPA	SPL
EE1	0.14	0.27	-0.01	0.23	0.31
EE2	-0.09	-0.24	-0.18	0.24	-0.12
EE3	-0.02	0.05	0.04	0.05	0.06

EE4	-0.02	0.10	0.03	0.18	0.18
EE5	-0.14	0.27	0.16	0.33	-0.08
EE6	0.11	0.03	0.07	0.26	0.20
<i>Echo vs no echo</i>	A1	V1	PHPA	OPA	SPL
EE1	0.19	0.16	0.27	0.06	0.11
EE2	0.02	0.48	0.14	0.20	-0.09
EE3	0.09	0.27	-0.08	0.14	0.14
EE4	0.10	0.32	0.01	0.54	0.31
EE5	-0.11	0.71	0.17	0.82	0.29
EE6	-0.07	0.73	0.33	0.56	0.58
<i>Sound vs silence</i>	A1	V1	PHPA	OPA	SPL
EE1	0.37	0.27	-0.09	0.24	0.25
EE2	0.30	0.10	0.20	0.10	-0.34
EE3	0.12	0.17	-0.09	0.01	0.01
EE4	0.15	0.27	-0.07	0.49	0.28
EE5	0.16	0.53	0.06	0.47	0.03
EE6	0.11	0.49	0.00	0.41	0.32

900

901

902

903

904

905

906 **Table 4**

907 Summary of peak activations within each cluster for the route vs. scrambled contrast.

908

Subject group	Cluster	Region label	MNI coords (mm)			z-stat	Num voxels
			x	y	z		
EEs	1	GM Superior parietal lobule 7P L (continuous with OPA)	-24	-72	28	3.14	899
	2	GM Inferior parietal lobule PGp R (continuous with OPA)	42	-82	20	3.21	325
BCs	n/a	n/a	n/a	n/a	n/a	n/a	n/a
SCs	1	GM Inferior parietal lobule PGp L	-18	-66	62	3.95	1370
		GM Superior parietal lobule 7A L					
		GM Superior parietal lobule 7P L					
	2	GM Broca's area BA44 L	-46	20	16	3.91	790
		GM Broca's area BA45 L					
		GM Premotor cortex BA6 L					
	3	Caudate	14	14	-4	3.85	423
	4	GM Anterior intra-parietal sulcus hIP3 R	28	-58	58	3.42	320
	GM Superior parietal lobule 7A R						
	GM Superior parietal lobule 7P R						

909

910

911 Table 5

912 As table 4, but for the echo vs. no echo contrast.

913

Subject group	Cluster	Region label	MNI coords (mm)			z-stat	Num voxels
			x	y	z		
EEs	1	GM Visual cortex V2 BA18 R	34	-88	22	4.51	11224
		GM Visual cortex V3V R					
	2	GM Premotor cortex BA6 R	40	-2	46	4.51	2163
		GM Anterior intra-parietal sulcus					
	3	hip3 L	-30	-58	54	4.09	1504
		GM Inferior parietal lobule Pfm L					
		GM Inferior parietal lobule Pga L					
	GM Superior parietal lobule 7A L						
BCs	4	GM Broca's area BA44 L	-50	8	28	4.07	1307
		GM Broca's area BA45 L					
	5	GM Premotor cortex BA6 R	-4	18	44	4.27	794
	6	Thalamus	-12	-14	0	3.36	731
	7	Temporal Lobe	-50	-48	12	4.12	622
	1	Cerebellum	52	-62	-12	4.23	6047
		Temporal Lobe					
	2	GM Broca's area BA45 L	-42	52	-4	4.49	3959
		GM Premotor cortex BA6 L					
	3	Frontal Lobe	30	26	0	4.64	3873
	4	GM Anterior intra-parietal sulcus	50	-40	58	4.59	2031

	hIP2 R					
	GM Anterior intra-parietal sulcus					
	hIP3 R					
	GM Inferior parietal lobule PF R					
	GM Inferior parietal lobule PFm R					
	GM Superior parietal lobule 7P R					
	GM Anterior intra-parietal sulcus					
5	hIP1 L	-32	-60	44	4.21	1880
	GM Anterior intra-parietal sulcus					
	hIP3 L					
	GM Inferior parietal lobule Pga L					
	GM Primary somatosensory cortex					
	BA2 L					
	GM Superior parietal lobule 7A L					
	GM Superior parietal lobule 7P L					
6	Frontal Lobe	-36	18	-2	4.3	938
	Insula					
	Putamen					
7	GM Inferior parietal lobule PFcm L	-50	-40	20	4.28	925
	GM Primary auditory cortex TE1.1 L					
8	GM Premotor cortex BA6 R	-4	20	44	5.13	791
9	GM Inferior parietal lobule PF R	66	-30	8	3.94	533
	GM Inferior parietal lobule PFcm R					
10	Putamen	20	12	-10	3.42	515
	Thalamus					

		Inferior Temporal Gyrus, temporooccipital part	-52	-54	8	3.75	308
		Lateral Occipital Cortex, inferior division					
		Middle Temporal Gyrus, temporooccipital part					
SCs	1	GM Broca's area BA44 R	46	8	24	5.96	10360
		GM Broca's area BA45 R					
		GM Anterior intra-parietal sulcus					
	2	hIP1 L	-46	-38	56	5.11	4597
		GM Inferior parietal lobule Pga L					
		GM Insula Id1 L					
		GM Primary somatosensory cortex BA1 L					
		GM Primary somatosensory cortex BA2 L					
		GM Anterior intra-parietal sulcus					
	3	hIP1 R	48	-38	52	5.45	3123
		GM Anterior intra-parietal sulcus					
		hIP2 R					
		GM Anterior intra-parietal sulcus					
		hIP3 R					
		GM Inferior parietal lobule PF R					
		GM Inferior parietal lobule PFm R					
		GM Inferior parietal lobule PFt R					

	GM Primary somatosensory cortex					
	BA1 R					
	GM Primary somatosensory cortex					
	BA2 R					
4	GM Inferior parietal lobule PF R	50	-32	8	4.73	2951
	GM Primary auditory cortex TE1.1 R					
5	GM Broca's area BA44 L	-58	6	28	5.31	2785
	GM Premotor cortex BA6 L					
6	Cerebellum	-10	-82	-30	5.62	1981
7	Thalamus	12	10	2	4.78	1121
8	Frontal Orbital Cortex	-36	28	2	4.77	805
	Frontal Pole					
	Insular Cortex					
9	Cerebellum	14	-78	-46	4.13	440

914

915

916

917 **Table 6**

918 As tables 4 and 5, but for the sound vs. silence contrast.

919

Subject group	Cluster	Region label	MNI coords (mm)			z-stat	Num voxels
			x	y	z		
EEs	1	GM Visual cortex V2 BA18 R	36	-90	6	4.2	7745
	2	GM Broca's area BA44 R	42	12	20	4.25	2636

		GM Broca's area BA45 R					
		GM Premotor cortex BA6 R					
		GM Anterior intra-parietal sulcus					
	3	hIP3 L	-34	-58	54	4.08	1987
		GM Superior parietal lobule 7A L					
		GM Superior parietal lobule 7P L					
	4	GM Premotor cortex BA6 R	6	26	42	4.04	728
		GM Inferior parietal lobule PFcm L					
		GM Primary auditory cortex TE1.0 L					
		GM Primary auditory cortex TE1.1 L					
		WM Acoustic radiation L					
	5	GM Inferior parietal lobule PFcm L	-50	-48	8	4.32	628
		GM Primary auditory cortex TE1.0 L					
		GM Primary auditory cortex TE1.1 L					
		WM Acoustic radiation L					
	6	GM Broca's area BA44 L	-58	12	22	3.86	539
		GM Premotor cortex BA6 L					
	7	GM Inferior parietal lobule PF R	62	-36	12	4.19	437
		GM Primary auditory cortex TE1.0 R					
		GM Primary auditory cortex TE1.1 R					
		WM Acoustic radiation R					
		GM Anterior intra-parietal sulcus					
BCs	1	hIP3 L	-42	-36	46	5.24	6653
		GM Primary somatosensory cortex					
		BA1 L					

	GM Primary somatosensory cortex					
	BA2 L					
	GM Primary somatosensory cortex					
	BA3b L					
2	Frontal Lobe	36	22	0	4.83	4237
	Insula					
	GM Anterior intra-parietal sulcus					
3	hIP2 R	42	-42	50	4.34	1370
	GM Anterior intra-parietal sulcus					
	hIP3 R					
	GM Inferior parietal lobule PF R					
	GM Inferior parietal lobule PFm R					
	GM Superior parietal lobule 7A R					
	GM Superior parietal lobule 7P R					
	GM Superior parietal lobule 7PC R					
4	GM Inferior parietal lobule PFcm L	-46	-38	18	4.31	1271
	GM Primary auditory cortex TE1.0 L					
	GM Primary auditory cortex TE1.1 L					
	GM Secondary somatosensory cortex					
	/ Parietal operculum OP1 L					
	WM Acoustic radiation L					
5	GM Inferior parietal lobule PF R	62	-34	12	5.15	1021
	GM Primary auditory cortex TE1.1 R					
	GM Secondary somatosensory cortex					
	/ Parietal operculum OP1 R					

		GM Secondary somatosensory cortex / Parietal operculum OP4 R					
		GM Anterior intra-parietal sulcus					
SCs	1	hIP1 L	-36	-28	10	6.57	8164
		GM Anterior intra-parietal sulcus					
		hIP3 L					
		GM Inferior parietal lobule PFcm L					
		GM Insula Ig1 L					
		GM Insula Ig2 L					
		GM Primary auditory cortex TE1.1 L					
		GM Primary somatosensory cortex					
		BA2 L					
		WM Acoustic radiation L					
	2	GM Broca's area BA44 R	38	0	50	5.58	7588
	3	GM Primary auditory cortex TE1.0 R	46	-26	8	5.54	2377
		GM Primary auditory cortex TE1.1 R					
		WM Acoustic radiation R					
	4	GM Premotor cortex BA6 R	-2	32	40	5.27	2153
		GM Anterior intra-parietal sulcus					
	5	hIP1 R	38	-54	42	5.83	2123
		GM Anterior intra-parietal sulcus					
		hIP2 R					
		GM Anterior intra-parietal sulcus					
		hIP3 R					
		GM Inferior parietal lobule PFm R					

GM Inferior parietal lobule Pga R						
6	Frontal Lobe	-34	18	-2	4.94	1047
	Insula					
7	Cerebellum	-12	-78	-22	4.74	806

920

921

922

923

924

925

926

927

928

929

930

931

932

933

934

935

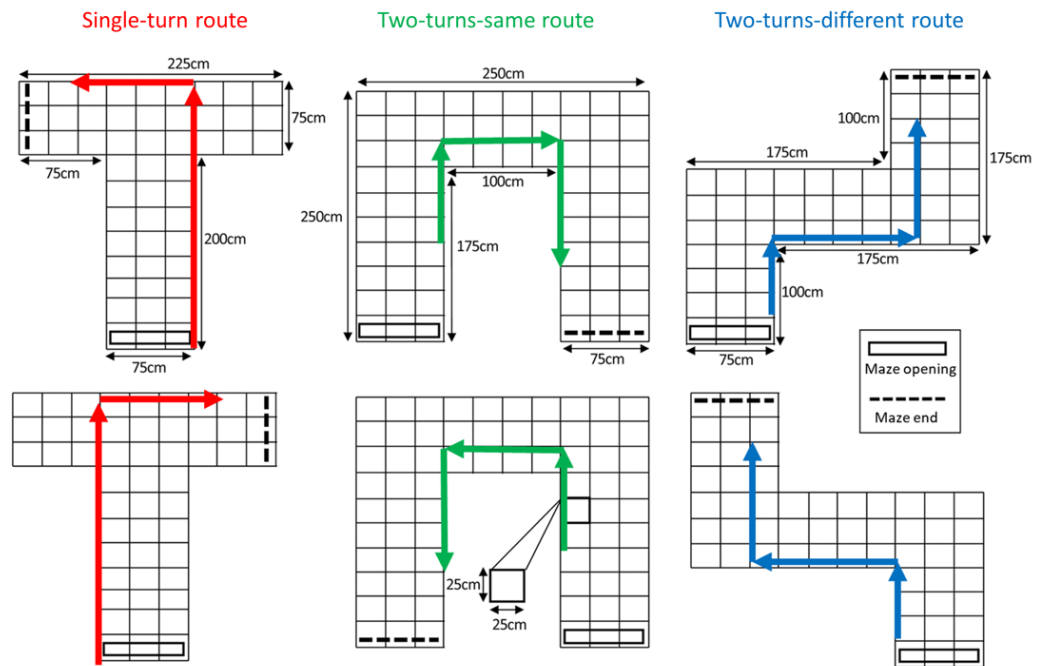
936

937

938

939

940 Figures



941

942 Figure 1

943 Illustration of spatial arrangements used to construct virtual spaces (T-mazes, U-mazes, Z-

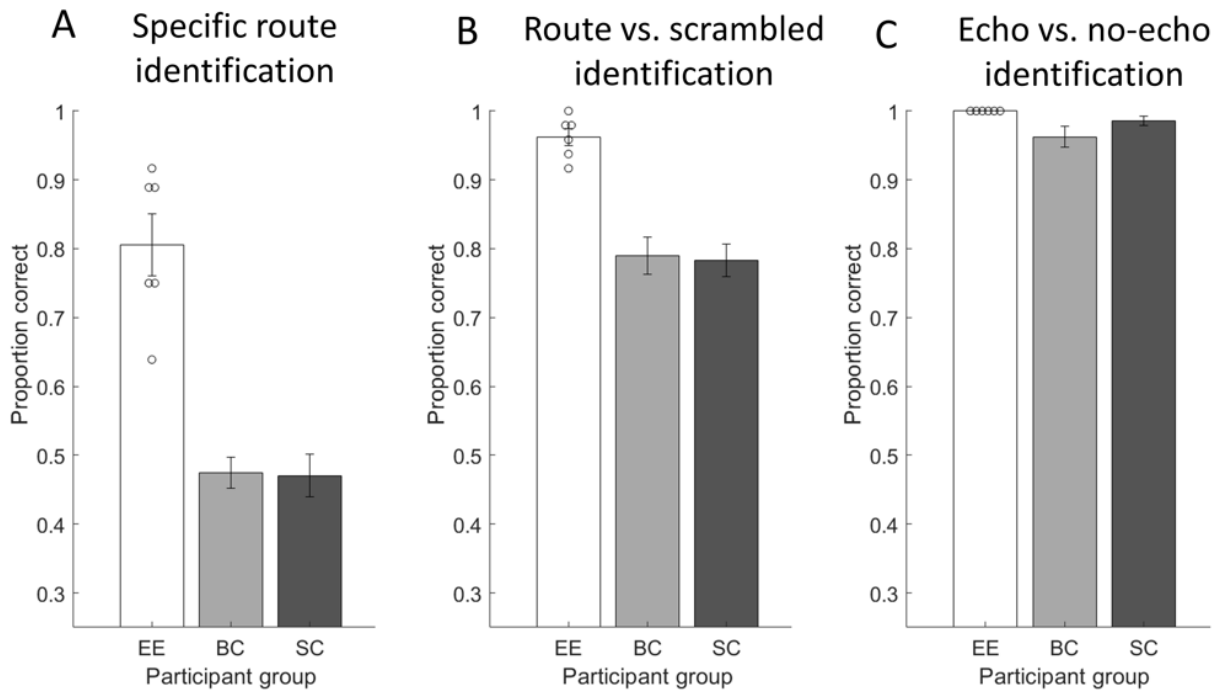
944 mazes) and the pre-specified routes taken through each one. Each route was composed of

945 18 click recordings taken at regularly spaced intervals. Specifically, there was one click for

946 each position along the route (marked by the intersections) and two clicks for each rotation

947 of 90° (in 45° steps).

948



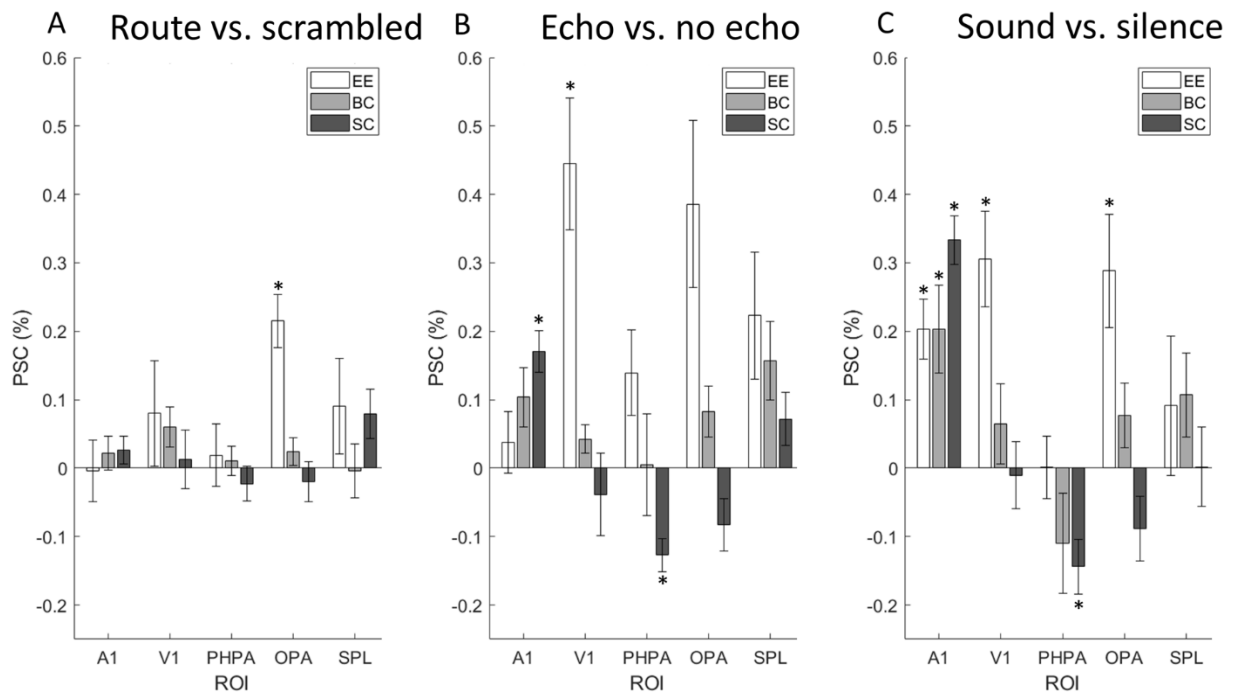
949

950 **Figure 2**

951 Data from the behavioural task conducted before the fMRI task. Three separate measures of
 952 performance are given: ability of participants to identify specific route types (A), to identify
 953 coherent route sounds vs. scrambled sounds (B), and to identify the sounds containing
 954 echoes from those that do not (C). Error bars show standard error of the mean. Circles
 955 illustrate performance of individual EEs. EE – Expert Echolocator; BC – Blind Control; SC –
 956 Sighted Control.

957

958



959

960 **Figure 3**

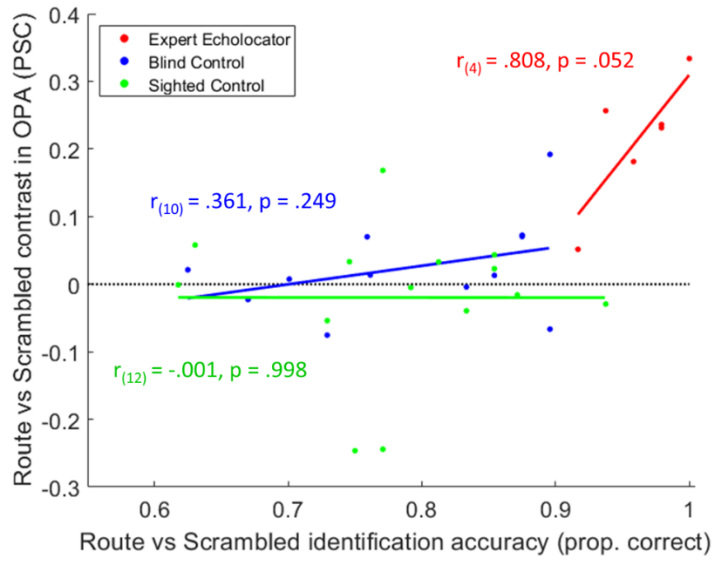
961 Results of the ROI analysis for route vs scrambled (A), echo vs no echo (B), and sound vs
 962 silence (C) contrasts. In each panel, percent signal change (PSC) is shown for each contrast,
 963 ROI and for participant group. Error bars show standard error of the mean. Asterisks
 964 indicate where the PSC for that ROI was significantly different from zero, after applying the
 965 Benjamini-Hochberg method. See also table 3 for the individual data for the six EEs.

966

967

968

969



970

971 **Figure 4**

972 The association between the PSC in OPA for the route vs scrambled contrast (y axis) and

973 perceptual identification accuracy of route vs scrambled sounds (x axis). Each point

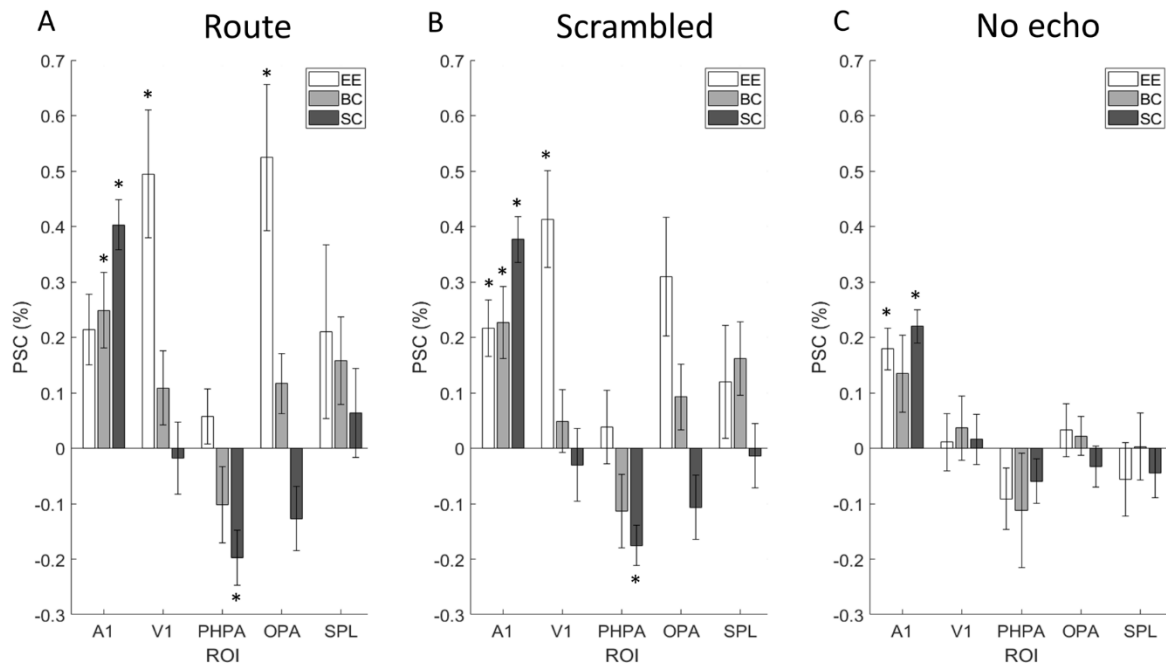
974 represents an individual subject, with separate groups denoted by different colours. The

975 solid lines show linear model fits.

976

977

978



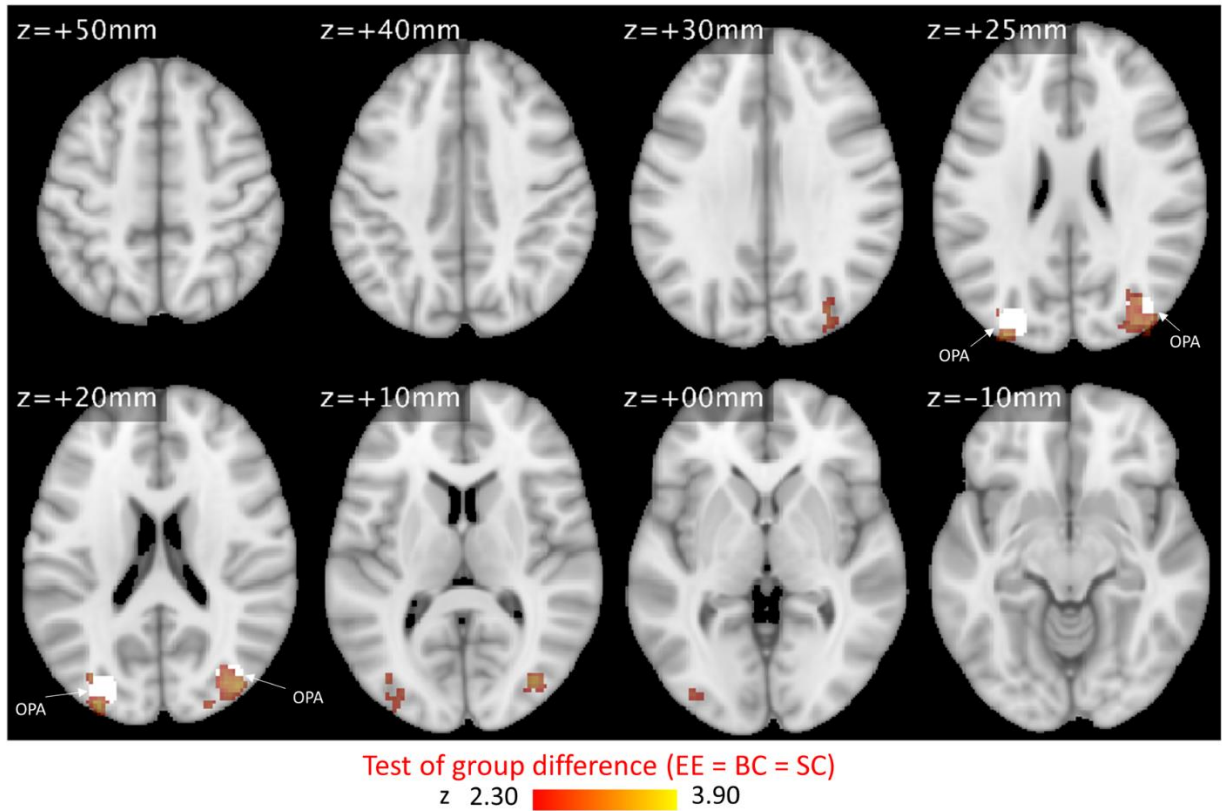
979

980 **Figure 5**

981 Results of the ROI analysis for the individual stimulus conditions (i.e. EVs relative to silence
 982 baseline): route sound (A), scrambled sound (B), and no echo sound (C). In each panel,
 983 percent signal change (PSC) is shown for each contrast, ROI and for participant group.
 984 Asterisks indicate where the PSC for that ROI was significantly different from zero, after
 985 applying the Benjamini-Hochberg method.

986

987



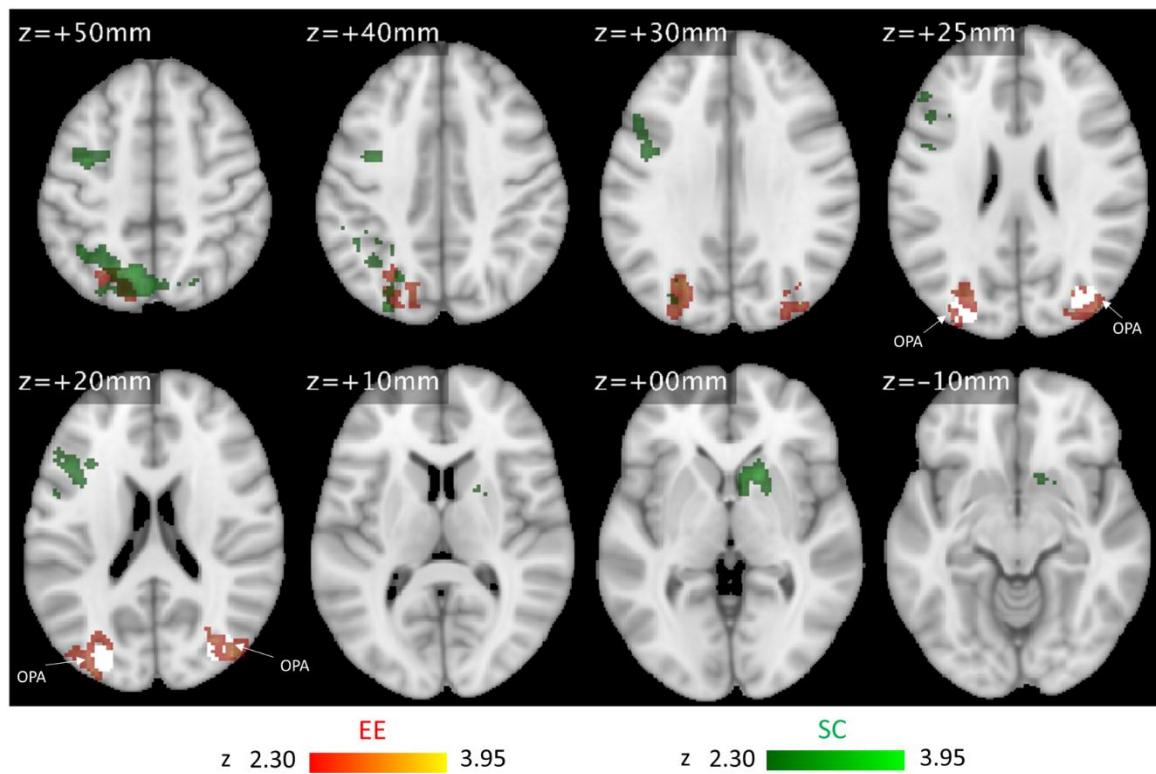
988

989 **Figure 6**

990 Activation maps showing locations of significant group difference for the contrast route vs.

991 scrambled (cluster level threshold of $z > 2.3$ and $p < .05$) displayed on the MNI152 standard-992 space template. The OPA ROI is visible in white in the cross-sectional slices for $Z = +20$ and993 $+25$ mm. Orientation of the images is in neurological convention (i.e. left is left).

994



995

996 **Figure 7**997 Activation maps for the contrast route vs. scrambled (cluster level threshold of $z > 2.3$ and $p <$ 998 $.05$) displayed on the MNI152 standard-space template. Separate colour overlays are used to

999 show results from EEs, BCs, and SCs on the (note there were no significant clusters for BCs).

1000 The colormap used to display each overlay is scaled such that they all have the same upper

1001 bound (determined by the largest z value in all three overlays). The OPA ROI is visible in1002 white in the cross-sectional slices for $Z = +20$ and $+25$ mm. Orientation of the images is in

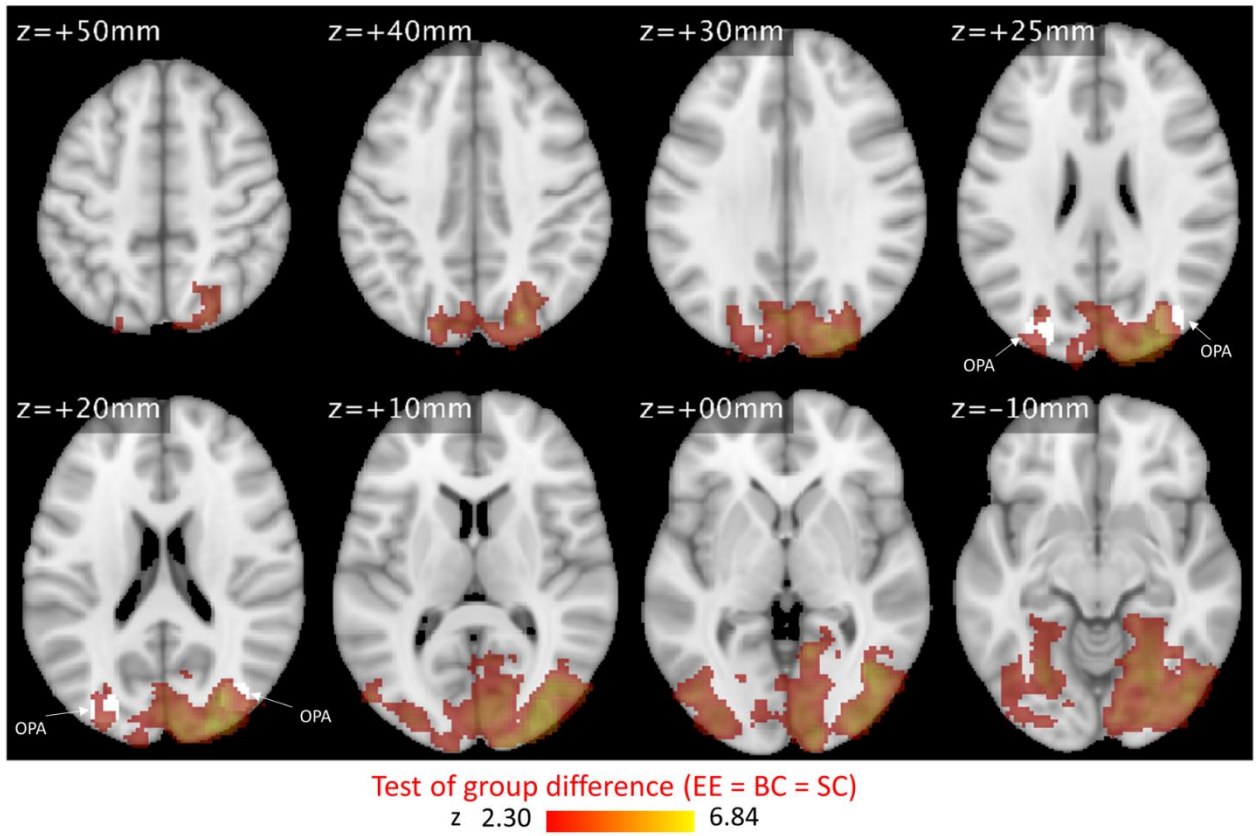
1003 neurological convention (i.e. left is left).

1004

1005

1006

1007



1008

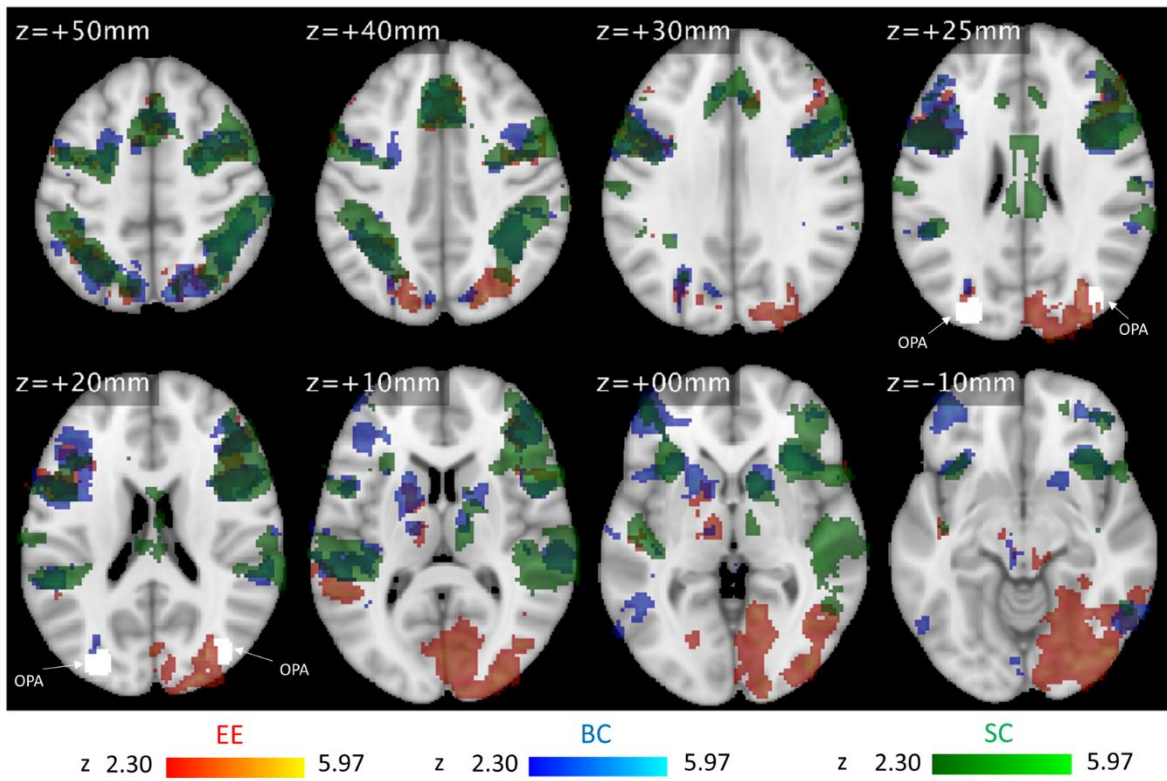
1009 **Figure 8**

1010 As figure 6, but for the contrast echo vs. no echo.

1011

1012

1013



1014

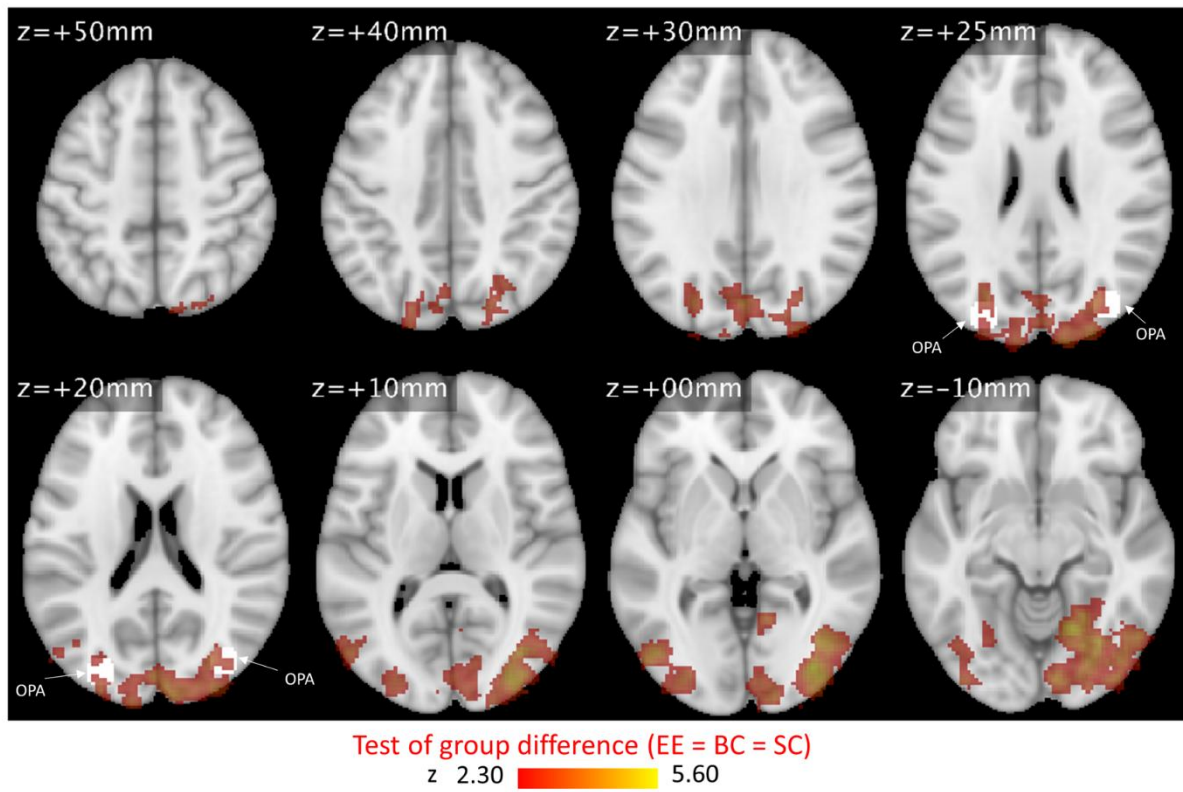
1015 **Figure 9**

1016 As figure 7, but for the contrast echo vs. no echo.

1017

1018

1019



1020

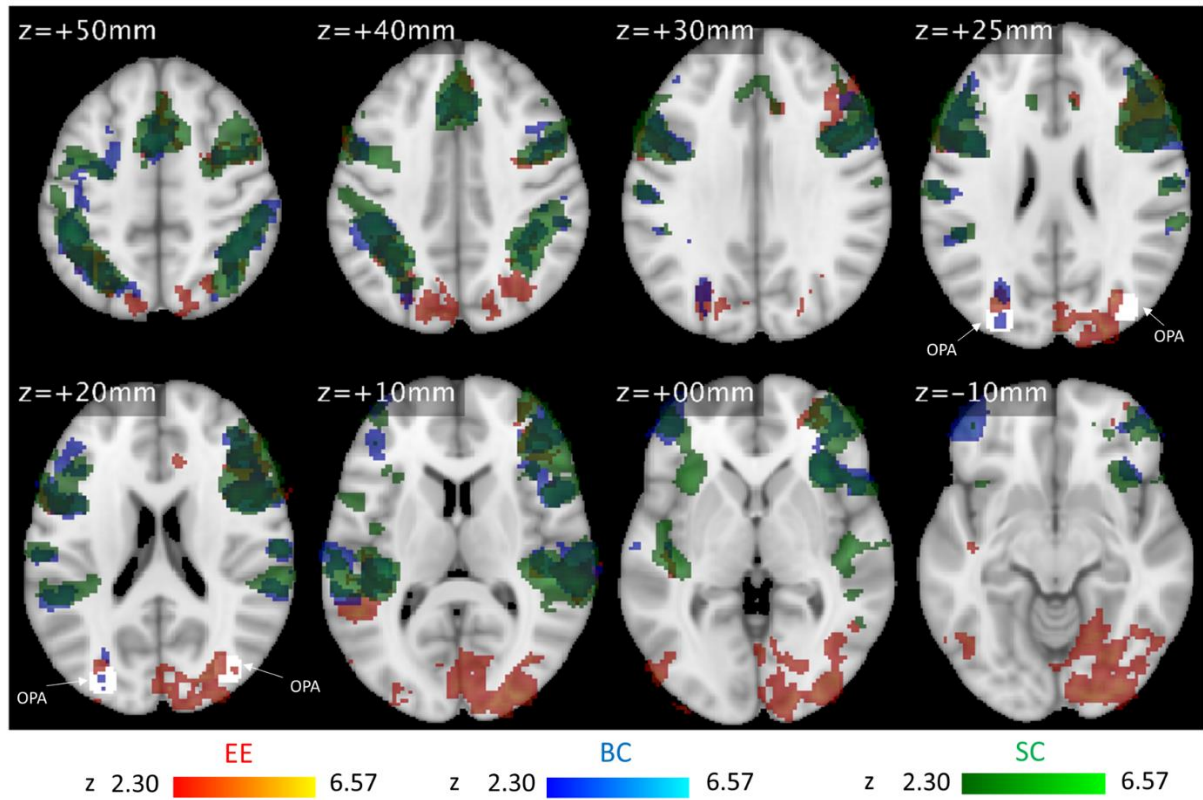
1021 **Figure 10**

1022 As figures 6 and 8, but for the contrast sound vs. silence.

1023

1024

1025



1026

1027 **Figure 11**

1028 As figures 7 and 9, but for the contrast sound vs. silence.

1029

1030

1031

1032

1033

1034

1035

1036

1037

1038